molecular pharmaceutics

Article

pubs.acs.org/molecularpharmaceutics

Formulation of Acid-Sensitive Micelles for Delivery of Cabazitaxel into Prostate Cancer Cells

Omer Aydin,[†,‡] Ibrahim Youssef,[†,‡,§] Yasemin Yuksel Durmaz,[†,∥] Gopinath Tiruchinapally,[†] and Mohamed E. H. ElSayed*[,†,⊥]

[†]Cellular Engineering & Nano-Therapeutics Laboratory, Department of Biomedical Engineering, College of Engineering, University of Michigan, Ann Arbor, Michigan 48109, United States

[§]Department of Chemistry, Faculty of Science, Mansoura University, Mansoura ET-35516, Egypt

[∥]Department of Biomedical Engineering, School of Engineering and Natural Sciences, Istanbul Medipol University, Istanbul, 34810, Turkey

[⊥]Macromolecular Science and Engineering Program, University of Michigan, Ann Arbor, Michigan 48109, United States

Supporting Information

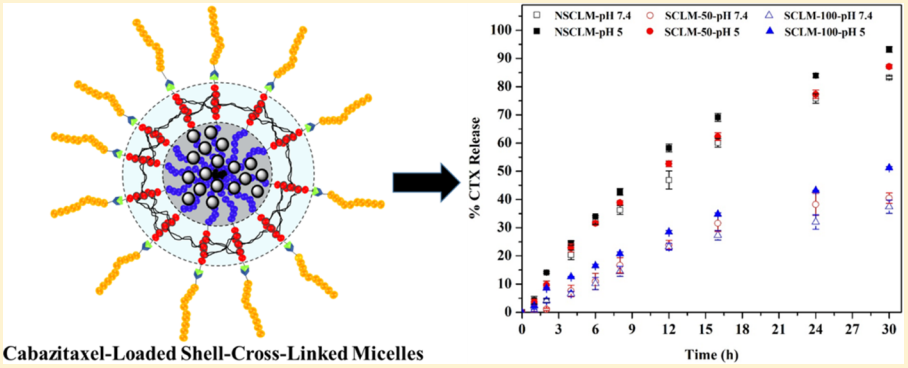

ABSTRACT: We report the synthesis of an amphiphilic triblock copolymer composed of a hydrophilic poly(ethylene glycol) (PEG) block, a central poly(acrylic acid) (PAA) block, and a hydrophobic poly(methyl methacrylate) (PMMA) block using atom transfer radical polymerization technique. We examined the self-assembly of PEG-*b*-PAA-*b*-PMMA copolymers in aqueous solutions forming nanosized micelles and their ability to encapsulate hydrophobic guest molecules such as Nile Red (NR) dye and cabazitaxel (CTX, an anticancer drug). We used 2,2β'-(propane-2,2-diylbis(oxy))-diethanamine to react with the carboxylic acid groups of the central PAA block forming acid-labile, shell cross-linked micelles (SCLM). We investigated the loading efficiency and release of different guest molecules from non-cross-linked micelles (NSCLM) and shell cross-linked micelles (SCLM) prepared by reacting 50% (SCLM-50) and 100% (SCLM-100) of the carboxylic acid groups in the PAA in physiologic (pH 7.4) and acidic (pH 5.0) buffer solutions as a function of time. We examined the uptake of NR-loaded NSCLM, SCLM-50, and SCLM-100 micelles into PC-3 and C4-2B prostate cancer cells and the effect of different micelle compositions on membrane fluidity of both cell lines. We also investigated the effect of CTX-loaded NSCLM, SCLM-50, and SCLM-100 micelles on the viability of PC-3 and C4-2B cancer cells compared to free CTX as a function of drug concentration. Results show that PEG-*b*-PAA-*b*-PMMA polymers form micelles at concentrations ≥11 μg/mL with an average size of 40−50 nm. CTX was encapsulated in PEG-*b*-PAA-*b*-PMMA micelles with 55% loading efficiency in NSCLM. *In vitro* release studies showed that 30% and 85% of the loaded CTX was released from SCLM-50 micelles in physiologic (pH 7.4) and acidic (pH 5.0) buffer solutions over 30 h, confirming micelles' sensitivity to solution pH. Results show uptake of NSCLM and SCLM into prostate cancer cells delivering their chemotherapeutic cargo, which triggered efficient cancer cell death. PEG-*b*-PAA-*b*-PMMA micelles were not hemolytic and did not cause platelet aggregation, which indicate their biocompatibility.

KEYWORDS: *amphiphilic polymers, acid-sensitive micelles, acid-labile linkers, cabazitaxel controlled release, prostate cancer, drug delivery*

1. INTRODUCTION

Taxanes are a family of hydrophobic, small molecular weight, drug molecules that include paclitaxel, docetaxel, and cabazitaxel, which exhibit cytotoxic activity against rapidly proliferating cancer cells.[1] Taxanes exhibit their cytotoxicity by

Received: February 21, 2016
Accepted: March 15, 2016
Published: March 15, 2016

DOI: 10.1021/acs.molpharmaceut.6b00147
Mol. Pharmaceutics 2016, 13, 1413−1429

blocking cell cycle progression through stabilizing the microtubules, centrosomal impairment, induction of abnormal spindles, and suppression of spindle microtubule dynamics, which triggers apoptosis by aberrant mitosis or by subsequent multinucleated G1-like state related to mitotic slippage depending on cell type and drug schedule.[2] The FDA approved the use of paclitaxel (Taxol, Bristol-Myers Squibb, Princeton, NJ) for treatment of ovarian cancer[3] and recurrent and metastatic breast cancer,[4] and as a second line therapy for patients with HIV-related Kaposi's sarcoma and non-small-cell lung carcinoma.[5,6] The FDA also approved the use of docetaxel (Taxotere, Sanofi-Aventis LLC, Bridgewater, NJ) for treatment of advanced breast,[7] lung,[8] and ovarian cancer.[9] However, clinical use of taxanes is associated with significant side effects including hypersensitivity reactions, neurotoxicity, bone marrow suppression, fluid retention (i.e., edema, ascites, pleural effusions), diarrhea, nausea, vomiting, numbness, and loss of hair due to the nonspecific distribution to healthy tissues.[10,11] Further, the use of surfactants such as Cremophor and polysorbate 80 to increase the intrinsically poor aqueous solubility of taxanes (e.g., paclitaxel's and docetaxel's solubility = 0.7 μg/mL and 6−7 μg/mL, respectively) has been shown to enhance the toxicity of the parent drug by causing allergic reactions, peripheral edema, and pericardial effusions.[12−14] Alternative formulations such as drug-loaded liposomes, albumin-based nanoparticles, polymer−drug conjugates, and self-assembled micelles have been developed to eliminate the need for toxic solubilizing agents and to target the loaded chemotherapeutic cargo to cancer cells.[15−18] Many of these strategies proved successful in enhancing the therapeutic activity of the loaded anticancer drug and reducing the associated toxicity in clinical settings, leading to the development and clinical use of Abraxane (paclitaxel-loaded albumin nanoparticles) for treatment of breast, lung, and pancreatic cancer[19,20] and Opaxio (polyglutamic acid−paclitaxel conjugate), which is being evaluated in phase III trials in patients with advanced ovarian cancer (NCT00108745).[21]

CTX is a chemotherapeutic agent that proved effective in killing resistant prostate cancer cells *in vitro* and in preclinical animal models.[22] These results led to FDA approval of cabazitaxel (Jevtana, Sanofi-Aventis LLC, Bridgewater, NJ) as a new treatment option for patients with castrate-resistant prostate cancer (CRPC) whose disease progresses during or after docetaxel treatment.[23−25] Activity of CTX in CRPC is attributed to its poor affinity for the ATP-dependent P-glycoprotein (P-gp) efflux pump compared to docetaxel, which is a strong substrate for P-gp.[26,27] Given that CTX is a lipophilic, practically insoluble in water, and chemically unstable drug,[28] it is formulated as lyophilized powder in single-use vials containing 60 mg of anhydrous CTX and 1.56 g of the polysorbate 80 surfactant to aid its dissolution when mixed with the appropriate diluent made of 13% (w/w) ethanol in water.[29] Preparation of CTX for infusion into CRPC patients requires two dilutions, and the use of polysorbate 80 as a solubility enhancer increases the risk for development of side effects, particularly hypersensitivity reactions including generalized erythema, hypotension, and bronchospasm.[30] We are interested in developing surfactant-free, water-soluble, and stable formulations of CTX that can be eventually targeted toward cancer cells in both the primary tumor (i.e., prostate gland) and distant metastases (e.g., cancer lesions in bone). To achieve this goal, we focused on the development of water-soluble nanosized micelles that can encapsulate CTX in their core, shuttle the CTX cargo into the cytoplasm of aggressive prostate cancer cells, and trigger efficient cancer cell death.

We report the synthesis of a new amphiphilic triblock copolymer composed of a hydrophilic poly(ethylene glycol) (PEG) block, a central poly(acrylic acid) (PAA) block, and a hydrophobic poly(methyl methacrylate) (PMMA) block. We evaluated the ability of poly(ethylene glycol-*b*-acrylic acid-*b*-methyl methacrylate) (PEG-*b*-PAA-*b*-PMMA) copolymer to self-assemble into micelles that encapsulate NR (a hydrophobic fluorescent dye) and CTX in the hydrophobic core. We report the synthesis of the acid-labile 2,2′-(propane-2,2-diylbis(oxy)-diethanamine linker and its reaction with the carboxylic acid groups in the central PAA block to cross-link adjacent polymer chains forming shell cross-linked micelles (SCLM). We compared the release of the loaded cargo (i.e., NR and CTX) from un-cross-linked micelles (NSCLM) and SCLM upon incubation in aqueous buffer solutions with physiologic (pH = 7.4) and endosomal (pH = 5.0) pH values. We investigated the uptake of CTX-loaded SCLM and NSCLM into PC-3 and C4-2B prostate cancer cells and the associated anticancer activity compared to free CTX at different drug concentrations. We evaluated micelle's biocompatibility by measuring the hemolysis of red blood cells (RBCs) and platelet aggregation upon incubation with different micelle concentrations. We also measured the adsorption of bovine serum albumin (BSA) as a model serum protein to the surface of SCLM and NSCLM as a function of incubation time and subsequent uptake of opsonized micelles by THP-1 macrophages.

2. EXPERIMENTAL SECTION

2.1. Materials. Cabazitaxel (CTX) is a generous gift from Sanofi-Aventis US LLC (Bridgewater, NJ). Poly(ethylene glycol) monomethyl ether (PEG, M_n: 5000 g/mol, Sigma-Aldrich), copper(I) bromide (CuBr, Sigma-Aldrich, 99.9%), anhydrous tetrahydrofuran (THF, Sigma-Aldrich, >99.9%), triethylamine (TEA, Sigma-Aldrich, ≥99%), *N*,*N*′- dicyclohexylcarbodiimide (DCC, Sigma-Aldrich, 99%), *N*-(2-hydroxyethyl)phthalimide (Sigma-Aldrich, 99%), 1,6-diphenyl-1,3,5-hexatriene (DPH, Sigma-Aldrich, 98%), resazurin sodium salt (Sigma-Aldrich), 2-methoxypropene (Sigma-Aldrich, 97%), phorbol myristate acetate (PMA, Sigma-Aldrich, ≥99%), benzene (anhydrous, Sigma-Aldrich, 99.8%), 2-propanol (anhydrous, Sigma-Aldrich, 99.5%), *p*-toluenesulfonic acid (Sigma-Aldrich, ≥98.5%), 4-pentynoic acid (Sigma-Aldrich, 99%), α-bromoisobutyryl bromide (Sigma-Aldrich, 98%), adenosine 5′-diphosphate (ADP, Sigma-Aldrich, ≥95%), *N*-hydroxy succinimide (NHS, Fluka, 97%), *N*-(3-(dimethylamino)propyl)-*N*′-ethylcarbodiimide hydrochloride (EDC, Fluka, >98%), dimethylaminopyridine (DMAP, Acros, 99%), sodium azide (NaN_3, Acros, 99%), trifluoroacetic acid (TFA, Acros, 99%), Nile Red (TCI AMERICA, Portland, OR), and Tween 20 (EMD Chemicals, Billerica, MA) were used as delivered without further purification. Methyl methacrylate (Sigma-Aldrich, MMA, 99%), *tert*-butyl acrylate (Sigma-Aldrich, *t*BA, 98%), and *N*,*N*,*N*′,*N*″,*N*″-pentamethyldiethylenetriamine (PMDETA, Sigma-Aldrich, 99%) were first purified by passing through a basic alumina column to remove the added inhibitor before using.

2.2. Instruments. A 500 MHz Varian Mercury system (Palo Alto, CA) was used to record all the ^{1}H NMR and ^{13}C NMR spectra of polymer blocks, the acid-labile linker, and the micelles at room temperature. Gel permeation chromatography (GPC) analysis was done using a Viscotek GPCmax

DOI: 10.1021/acs.molpharmaceut.6b00147
Mol. Pharmaceutics 2016, 13, 1413−1429

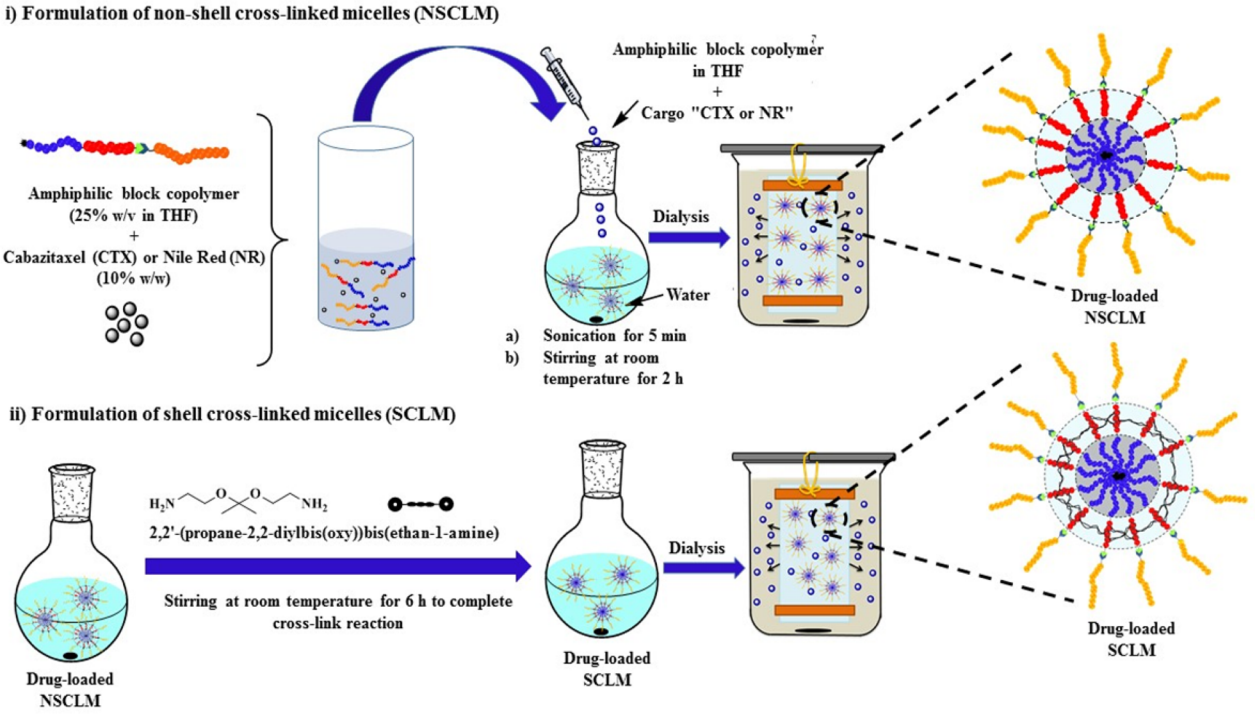

Figure 1. (A) Scheme for the synthesis of PEG-*b*-PAA-*b*-PMMA copolymers. (B) A schematic drawing showing the formulation of PEG-*b*-PAA-*b*-PMMA polymers into NR- and CTX-loaded NSCLM and SCLM micelles.

Autosampler system consisting of a pump and Waters 2414 refractive index (RI) detector. The molecular weight and molecular weight distribution of synthesized polymers were determined based on their elution volume on a Styragel HR 4E column compared to a series of poly(methyl methacrylate) standards (PolyAnalitik Inc., Canada) using THF as a mobile phase at a flow rate of 1 mL/min at 35 °C. The data was analyzed using Viscotek OmniSEC Omni-01 software. PerkinElmer FT-IR Spectrum 4100 type A machine was used to confirm the azidation of different polymer blocks. The 90Plus particle size analyzer (Brookhaven Instruments Corporation, Holtsville, NY) was used to measure micelles' size and surface charge. The JEOL 3011 high resolution electron microscope (JEOL USA Inc., Peabody, MA) was used to image micelles' morphology.

2.3. Synthesis of Amphiphilic PMMA-*b*-PAA-*b*-PEG Copolymer. Amphiphilic PMMA-*b*-PAA-*b*-PEG triblock copolymer was synthesized by a combination of atom transfer radical polymerization (ATRP) technique and "click" coupling reactions (Figure 1A). Briefly, the hydrophobic PMMA block was synthesized using the ATRP technique[31] and utilized as a macro initiator for copolymerization of *tert*-butyl acrylate (*t*BA) to obtain the PMMA-*b*-P*t*BA-Br copolymer. The bromine (Br) end groups were converted to azide (N_3) to allow "click" coupling to the alkyne-functionalized PEG block forming the (PMMA-*b*-P*t*BA-*b*-PEG) copolymer. Acid hydrolysis was used to remove the *tert*-butyl groups in the central P*t*BA block and obtain the desired (PMMA-*b*-PAA-*b*-PEG) copolymer.

2.3.1. Synthesis of the Hydrophobic PMMA Block. The hydrophobic PMMA block was synthesized by ATRP following published protocols.[32] Briefly, the MMA monomer (30 mL, 282 mmol), CuBr catalyst (202 mg, 1.41 mmol), *N*,*N*,*N*′,*N*′,*N*″-pentamethyldiethylenetriamine (PMDETA) ligand (294 mg, 1.41 mmol), ethyl-2-bromoisobutyrate initiator (207 μL, 1.41 mmol), and 30 mL of toluene were introduced into a Schlenk tube, and the reaction mixture was degassed by three freeze−pump−thaw cycles. The tube was then placed in a temperature-controlled oil bath at 40 °C for 21 min. The polymerization mixture was diluted with THF and passed through a neutral alumina column to remove the copper complex. THF was removed by rotary evaporation, and the mixture was precipitated in hexane. Results show that 30% of MMA monomers were converted into PMMA block with $M_{n,theo}$ = 4855 g/mol, $M_{n,NMR}$ = 4400 g/mol, $M_{n,GPC}$ = 4855 g/mol, and M_w/M_n = 1.27. ^{1}H NMR of the PMMA block (500 MHz, $CDCl_3$, δ) shows: 4.21 (2H, $CH_3-CH_2-O-CO-C(CH_3)_2$), 3.57 (s, 3H, CH_3-O-CO), 1.95 (2H, $CH_2-C(CH_3)-CO$), 1.85 (6H, $O-CO-C(CH_3)_2$), 1.22 (3H, $CH_3-CH_2-O-CO-C(CH_3)_2$) (Figure S1).

2.3.2. Synthesis of Azide-Functionalized PMMA-b-PtBA-N_3 Copolymer. The PMMA block was used as a macro initiator for block copolymerization with *tert*-butyl acrylate to obtain PMMA-*b*-P*t*BA block copolymer. Briefly, PMMA (2.22 g, 0.5 mmol), CuBr (72 mg, 0.5 mmol), PMDETA (104 μL, 0.5 mmol), *t*BA (7.32 mL, 50 mmol), and 18.3 mL of toluene were introduced into a Schlenk tube and the reaction mixture was degassed by three freeze−pump−thaw cycles. The tube was then placed in a temperature-regulated oil bath at 80 °C for 6 h. The reaction mixture was diluted with THF before passing through a neutral alumina column to remove the copper complex, THF was removed by rotary evaporation, and the mixture was precipitated in cold methanol/water (80/20 v/v). $M_{n,NMR}$: 8000 g/mol. $M_{n,GPC}$: 9596 g/mol. M_w/M_n: 1.23. ^{1}H NMR of the PMMA-*b*-P*t*BA-Br polymer (500 MHz, $CDCl_3$, δ) shows: 4.05 (2H, CH_3-CH_2-O-CO, and 1H, $CH_2-CH-Br$), 3.56 (s, 3H, $CO-O-CH_3$), 2.24 (CH_2CH-CO), 1.86−0.82 (6H, $O-CO-C(CH_3)_2$, $CO-O-C(CH_3)_3$, CH_2-CCH_3) (Figure S2).

The terminal Br groups in PMMA-*b*-PtBA-Br polymer were converted to azide by reacting with excess NaN_3 to allow "click"

DOI: 10.1021/acs.molpharmaceut.6b00147
Mol. Pharmaceutics 2016, 13, 1413−1429

coupling to the alkyne-functionalized PEG block. Briefly, PMMA-*b*-P*t*BA-Br (1 g, 1.25×10^{-1} mmol) and 20 equiv of NaN_3 (0.16 g, 2.5 mmol) were stirred together in DMF overnight at 50 °C. The polymer was dissolved in CH_2Cl_2 and extracted with water, followed by reverse extraction of the water phase with CH_2Cl_2, combining the organic layers, and drying over Na_2SO_4. Finally, the organic layer was evaporated to obtain the PMMA-*b*-P*t*BA-N_3 Polymer. $M_{n,GPC}$ = 10 073 g/mol, M_w/M_n = 1.18. ^{1}H NMR (500 MHz, $CDCl_3$, δ) shows: 4.05 (2H, CH_3-CH_2-O-CO), 3.77 (CH_2CH-N_3), 3.58 (s, $CO-O-CH_3$), 2.26 ($CH_2-CH-CO$), 1.93–0.83 (6H, $O-CO-C(CH_3)_2$, $CO-O-C(CH_3)_3$, CH_2-CCH_3) (Figure S3).

2.3.3. Synthesis of Alkyne-Functionalized Poly(ethylene glycol) (PEG-Alkyne). PEG (M_n: 5000 g/mol) with monohydroxyl functional end group (5 g, 1.0 mmol), 4-pentynoic acid (147 mg, 1.5 mmol), *N*,*N*′-dicyclohexylcarbodiimide (DCC) (206 mg, 1.0 mmol), 4-dimethylaminopyridine (DMAP) (122 mg, 1.0 mmol), and 25 mL of dichloromethane (DCM) were introduced into a round-bottom flask and stirred overnight at room temperature. After filtration of the formed salts, the reaction mixture was concentrated by rotary evaporation and the PEG polymer was precipitated three times in diethyl ether followed by filtration. The yield was 3.80 g (76%) with 94% functionalization efficiency. ^{1}H NMR (500 MHz, $CDCl_3$, δ): 4.26 (t, 2H, $CO-O-CH_2$), 3.71 (t, 2H $CO-O-CH_2-CH_2-O$), 3.65 (bs, 450H, $O-CH_2-CH_2$), 3.38 (s, 3H, $CH_2-CH_2-O-CH_3$), 2.58 (2H, CH_2-CH_2-CO-O), 2.51 (2H, CH_2-CH_2-CO-O), 1.99 (1H, alkyne proton) (Figure S4).

2.3.4. "Click" Coupling of PMMA-b-PtBA-N_3 and PEG-Alkyne Blocks. PEG-alkyne (447 mg, 8.78×10^{-2} mmol, 1 equiv), PMMA-*b*-P*t*BA-N_3 (710 mg, 9.66×10^{-2} mmol, 1.1 equiv), CuBr (15.1 mg, 1.05×10^{-1} mmol, 1.2 equiv), PMDETA (21.9 μL, 1.05×10^{-1} mmol, 1.2 equiv), and 6 mL of DMF were introduced into a Schlenk tube, and the reaction mixture was degassed by three freeze–pump–thaw cycles before the tube was placed in an oil bath at room temperature for 48 h. The reaction mixture was diluted with THF and passed through a neutral alumina column to remove the copper complex, and the polymer was precipitated twice in diethyl ether and a third time in methanol before being collected by centrifugation. The polymer product was dissolved in DCM and precipitated several times in a DCM/hexane mixture to remove unreacted PEG following a published protocol.[32] The molecular weight and molecular weight distribution of the PMMA-*b*-P*t*BA-*b*-PEG polymer are $M_{n,GPC}$ = 20 281 g/mol and M_w/M_n = 1.08. ^{1}H NMR (500 MHz, $CDCl_3$, δ) shows: 7.46 (bs, 1H, triazole ring proton), 4.25 (CH_2CH-triazole and $CO-O-CH_2$), 4.05 (2H, CH_3-CH_2-O-CO), 3.64 (bs, $O-CH_2-CH_2$), 3.59 (s, $CO-O-CH_3$), 3.38 (s, 3H, $CH_2-CH_2-O-CH_3$), 3.05 (2H, triazole$-CH_2-CH_2-CO-O$), 2.76 (2H, triazole$-CH_2-CH_2-CO-O$), 2.26 ($CH_2-CH-CO$), 1.93–0.83 (6H, $O-CO-C(CH_3)_2$, $CO-O-C(CH_3)_3$, CH_2-CCH_3) (Figure S5).

The *tert*-butyl groups in the central block were hydrolyzed using trifluoroacetic acid (TFA) to obtain the corresponding carboxylic acid. Briefly, the PMMA-*b*-P*t*BA-*b*-PEG polymer was dissolved in DCM followed by adding 10-fold TFA (compared to the molar concentration of the *tert*-butyl groups) at 0 °C under argon atmosphere. The reaction mixture was stirred for 30 min at 0 °C and allowed to stand stirring for 24 h at room temperature. DCM and TFA were evaporated with an air stream and the PMMA-*b*-PAA-*b*-PEG polymer was precipitated in methanol. $M_{n,GPC}$ = 14 860 g/mol and M_w/M_n = 1.15 for the PMMA-*b*-PAA-*b*-PEG polymer. ^{1}H NMR (500 MHz, $CDCl_3$, δ) showed complete loss of the *tert*-butyl protons at 1.45 ppm (Figure S6).

2.4. Synthesis of Acid-Labile 2,2′-(Propane-2,2-diylbis(oxy))-diethanamine Cross-Linker. The acid-labile 2,2′-(Propane-2,2-diylbis(oxy))-diethanamine cross-linker was synthesized following published methods.[33−37] Briefly, *N*-(2-hydroxyethyl)phthalimide (5.0 g, 26.15 mmol, 1 equiv) was completely dissolved in 100 mL of dry benzene and cooled down to 0 °C in an ice bath. 2-Methoxypropene (2.5 mL, 26.15 mmol, 1 equiv) was carefully added to the solution along with *p*-toluenesulfonic acid (50 mg, 0.78 mmol). The reaction mixture was stirred for 1.5 h while keeping the temperature at 0 °C to avoid loss of the highly volatile 2-methoxypropene. The flask was then connected to a trap, and the mixture was heated to 45 °C under high vacuum to remove the methanol formed during the reaction. Additional benzene was added and subsequently evaporated for 6 h before the reaction was quenched by adding triethylamine (6.67 mL) and allowing the reaction mixture to warm up to room temperature. Acetic anhydride (1.33 mL) was added to convert unreacted alcohol groups into the corresponding acetate, and the mixture was stirred overnight. The reaction mixture was then precipitated by dropwise addition to hexane. The precipitated powder was collected and recrystallized twice from ethyl acetate yielding a white solid. Reaction yield was 70%. ^{1}H NMR (500 MHz, $CDCl_3$, δ) shows: 1.3 (6H, s, CH_3-C), 3.6 (4H, t, CH_2-O), 3.80 (4H, t, CH_2-N), 7.4–7.8 (8H, dt, ArH) (Figure S7). Calculated $[M + H]^+$ ($C_{23}H_{22}N_2O_6$) m/z = 422.15 and found $[M + Na]^+$ = 445.1.

The formed 2,2′-(propane-2,2-diylbis(oxy))bis(diethane-2,1-diyl)bis(isoindoline-1,3-dione) (400 mg) was deprotected by refluxing overnight with 5 mL of 6 M NaOH to obtain 2,2′-(propane-2,2-diylbis(oxy))-diethanamine. The final product was extracted three times by a mixture of $CHCl_3$/iPrOH (1/1 v/v) and dried over anhydrous sodium sulfate before evaporating the organic layer to obtain an amber-colored oil. The reaction yield was 50%. ^{1}H NMR (500 MHz, $CDCl_3$, δ) shows: 1.36 (6H, s, CH_3-C), 1.44 (4H, bs, NH_2), 2.81 (4H, t, CH_2-NH_2), 3.45 (4H, t, CH_2-O). ^{13}C NMR (500 MHz, $CDCl_3$) δ (ppm for TMS): 24.98, 42.18, 62.88, and 99.79 (Figure 3A and 3C). Calculated $[M + H]^+$ ($C_7H_{19}N_2O_2$) m/z = 162.14 and found $[M + H]^+$ = 163.14 and $[M + Na]^+$ = 185.1.

2.5. Formulation of PMMA-*b*-PAA-*b*-PEG Polymers into Micelles. Amphiphilic PMMA-*b*-PAA-*b*-PEG polymer (10 mg, 8.66×10^{-4} mmol) was dissolved in 1.5 mL of THF by stirring for 5 min before being add dropwise to 15 mL of water in a sonicating water bath. After 2 h of stirring at room temperature, the solution mixture was transferred to a dialysis bag (MWCO 1 kDa), which was placed in a large water bath for 24 h. After 24 h of dialysis, the solution of un-cross-linked micelles (NSLCM) was lyophilized to obtain the corresponding powder. Micelle cross-linkage using the acid-labile 2,2′-(propane-2,2-diylbis(oxy))-diethanamine started by acidifying the NSCLM solution down to pH 4.0 by adding 1 N HCl followed by 150 μL of *N*-(3-(dimethylamino)propyl)-*N*′-ethylcarbodiimide hydrochloride (EDC) (8.28 mg, 4.32×10^{-2} mmol) and 150 μL of *N*-hydroxy succinimide (NHS) (2.49 mg, 2.16×10^{-2} mmol) in 100 mM 2-(*N*-morpholino)-ethanesulfonic acid (MES) solution and stirring for 3 h to form the NHS esters of the carboxylic acid groups in the central PAA block. The pH of the micelle solution was adjusted to 9.2 using

DOI: 10.1021/acs.molpharmaceut.6b00147
Mol. Pharmaceutics 2016, 13, 1413−1429

a 1 N NaOH solution before adding the 2,2′-(propane-2,2-diylbis(oxy))-diethanamine cross-linker and stirring the reaction mixture for 9 h at room temperature. By adjusting the amount of the 2,2′-(propane-2,2-diylbis(oxy))-diethanamine cross-linker added to the micelle solution, we cross-linked 50% or 100% of the NHS-activated carboxylic acid groups in the central PAA block to obtain shell cross-linked micelles (SCLM). Specifically, 0.44 mg, 0.27×10^{-2} mmol, or 0.88 mg, 0.54×10^{-2} mmol, of the 2,2′-(propane-2,2-diylbis(oxy))-diethanamine cross-linker was added to the NHS-activated NSCLM solution to prepare SCLM-50 (50% PAA cross-linkage density) or SCLM-100 (100% PAA cross-linkage density), respectively. After 9 h of stirring at room temperature, the reaction mixture was dialyzed against double distilled H_2O with pH 9.0 for 24 h before lyophilization.

NR- and CTX-loaded micelles were formulated following the same protocol. Briefly, PMMA-*b*-PAA-*b*-PEG polymer (15 mg, 8.66×10^{-4} mmol) was dissolved in 2.25 mL of THF by stirring for 5 min before adding the 10% w/w solution of NR or CTX and stirring for an additional 30 min at room temperature. This solution mixture was added dropwise into 22.5 mL of double distilled water while sonicating to trigger micelle formation followed by stirring for 2 h at room temperature to obtain a homogeneous solution of NR- or CTX-loaded NSCLM solution. A fraction of the NR- or CTX-loaded NSCLM solution was reacted with NHS/EDC to convert the carboxylic acid groups of the PAA block into the activated NHS ester before adding the 2,2′-(propane-2,2-diylbis(oxy))-diethanamine cross-linker following the same procedure described earlier to prepare SCLM. We controlled the amount of the cross-linker added to the reaction mixture to prepare NR- and CTX-loaded SCLM-50 and SCLM-100 micelles to investigate the effect of shell cross-linkage density on the loading and release of the NR and CTX cargo. NR- and CTX-loaded NSCLM were transferred to dialysis bags with a MWCO of 1 kDa and dialyzed against double distilled water containing Tween 80 (0.5% w/v) for 2 h to remove free NR and CTX from the micelle solution followed by dialysis against double distilled water for 24 h before lyophilization to obtain NR- and CTX-loaded NSCLM as dry powder. NR- and CTX-loaded SCLM-50 and SCLM-100 micelles were dialyzed against double distilled water with pH 9.0 for 24 h before lyophilization.

After lyophilization, 1 mg of the dry powder was dissolved in 10 mL of THF followed by measuring UV absorbance at 550 and 230 nm to quantify the amount of NR and CTX present in solution using concentration versus absorbance calibration curves (NR concentration range was 0−50 μM, and CTX concentration range was 0−300 μM). We calculated NR and CTX content in the dry micelles and their loading efficiency using the following equations.

$$\text{NR/CTX content (\% by wt)} = \frac{\text{calcd amount of NR or CTX in dry powder}}{\text{total wt of dry powder}} \times 100\% \quad (1)$$

$$\text{loading efficiency (\%)} = \frac{\text{calcd amount of NR or CTX in dry powder}}{\text{amount of NR or CTX used in micelle formulation}} \times 100\% \quad (2)$$

2.6. Micelle Characterization. The transition of PMMA-*b*-PAA-*b*-PEG polymer from unimers to micelles in aqueous solutions was investigated by monitoring the change in NR fluorescence upon increasing the polymer's concentration following a published protocol.[38] Specifically, self-assembly of the PMMA-*b*-PAA-*b*-PEG polymer into micelles and NR encapsulation in the hydrophobic core has been shown to increase its fluorescence signal, which was used to measure the critical micelle concentration (CMC) of this amphiphilic polymer. Briefly, PMMA-*b*-PAA-*b*-PEG polymer was dissolved in DI water at different concentrations ranging from 0.0001 to 0.6 mg/mL. A 0.1 mM stock solution of NR in THF was prepared, and 10 μL aliquots were transferred to glass vials and allowed to air-dry for 2 h at room temperature before adding 1 mL of different polymer solutions, mixing in a sonicating water bath for 1 h, and allowing to stand at room temperature for 2 h. The fluorescence intensity of NR in different polymer solutions was measured (λ_{ex} = 550 ± 2 nm, λ_{em} = 620 ± 2 nm) using a Fluoroskan Ascent FL plate reader (Thermo Fisher Scientific, Waltham, MA), which was plotted against polymer concentration to determine the CMC. Further, the size and zeta potential of empty and NR/CTX-loaded NSCLM, SCLM-50, and SCLM-100 micelles were measured using a 90Plus particle size analyzer with ZetaPALS capability (Brookhaven Instruments Corporation, Holtsville, NY) at 25 °C following established protocols.[39] The morphology of NSCLM was visualized using the JEOL 3011 high resolution electron microscope. Briefly, 1 mg of NSCLM micelles was dissolved in 1 mL of distilled water by mixing and 10 μL of the solution was placed on a 400 mesh grid (Ted Pella Inc., Redding, CA) before imaging at a magnification of 10000× under an accelerating voltage of 300 kV.

2.7. NR and CTX Release Studies. Release of NR and CTX from NSCLM, SCLM-50, and SCLM-100 was investigated as a function of solution pH and incubation time. Briefly, 1 mg of NR- and CTX-loaded NSCLM, SCLM-50, and SCLM-100 micelles was dissolved in 2 mL of PBS with pH 7.4 or 5.0 before transferring to dialysis cassettes (MWCO 3500 Da), which were immersed in 150 mL of PBS (pH 7.4) or acetate buffer (pH 5.0) containing 0.5% w/v Tween 20 and kept at 37 °C while stirring at 150 rpm. Release of NR from NR-loaded micelles was quantified by drawing four 200 μL samples from the release media after 0.5, 1, 1.5, 2, 2.5, 3, 3.5, 4, 4.5, 5, 5.5, 6, 6.5, 7, 7.5, 8, 10, 13, and 24 h from immersing the dialysis cassettes in the release solution followed by measuring NR fluorescence in the collected samples (λ_{ex} = 550 nm, λ_{em} = 620 nm) using the Fluoroskan plate reader. Similarly, release of CTX from CTX-loaded micelles was quantified by drawing four 200 μL samples from the release media after 1, 2, 4, 6, 8, 12, 14, 16, and 24 h from immersing the dialysis cassettes in the release solutions followed by measuring the amount of CTX in each sample using high pressure liquid chromatography (HPLC). Briefly, CTX solutions were analyzed using a C18 Ascentis Express column (Waters Corp., Milford, MA; 2.7 μm, 15 cm × 3.0 mm) connected to a Waters HPLC system equipped with a UV dual absorbance detector. A mixture of solvent A (650 mL of H_2O and 350 mL of ACN) and solvent B (250 mL of H_2O and 750 mL of ACN) was used as a mobile phase to resolve the released CTX on the C18 column starting with a gradient of solvent A:solvent B of 100:0 for 7 min, 62:38 for 29 min, 22:78 for 0.1 min, and 100:0 for 9 min at a flow rate of 0.6 mL/min while keeping the column at 40 °C throughout the analytical run. Absorbance of the eluting CTX molecules was measured at

DOI: 10.1021/acs.molpharmaceut.6b00147
Mol. Pharmaceutics 2016, 13, 1413−1429

230 nm. The total amount of the released CTX was calculated based on UV absorbance versus concentration calibration curve using the Waters Breeze software.

2.8. Cell Culture. PC-3 and C4-2B prostate cancer cells were a generous gift from Dr. Evan Keller (University of Michigan) and were cultured following published protocols.[40] Briefly, PC-3 cells were cultured in RPMI-1640 while C4-2B cells were cultured in T-medium, which were both supplemented with 10% fetal bovine serum (FBS; Gibco, Carlsbad, CA) and 1% antibiotic−antimycotic solution (Gibco, Carlsbad, CA). PC-3 and C4-2B cells were incubated at 37 °C and 5% CO_2 while changing the culture medium every other day and passaging the cells using 0.05% trypsin−EDTA solution after reaching 80% confluence. The passage number for PC-3 and C4-2B cells used in the uptake and cytotoxicity studies was in the range between 25 and 40.

HEK 293 human embryonic kidney cells were a generous gift from Dr. Rhima Coleman (University of Michigan) and were cultured in DMEM medium supplemented with 10% fetal bovine serum. The cells were incubated at 37 °C and 5% CO_2 while changing the culture medium every other day and passaging the cells using 0.25% trypsin−EDTA solution after reaching 80% confluence.

Nonadherent THP-1 acute monocytic leukemia cells were a generous gift from Dr. Katsuo Kurabayashi and Dr. Jianping Fu (University of Michigan), which were cultured in RPMI-1640 medium supplemented with 10% FBS and 120 μM β-mercaptoethanol. THP-1 cells were activated into phagocytic and adherent ones by seeding in 24-well plates at a seeding density of 200,000 cells/well followed by incubating with regular culture medium supplemented with 200 nM phorbol myristate acetate (PMA) for 3 days. Differentiated and adherent THP-1 cells were cultured for 5 more days in PMA free culture medium before being used in uptake studies. Both nonadherent and differentiated THP-1 cells were cultured in a humidified 5% CO_2 at 37 °C.

2.9. Cellular Uptake Studies. PC-3 and C4-2B human prostate cancer cells were seeded in 24-well plates at a seeding density of 2×10^5 cells/well and allowed to adhere for 24 h before incubating with free NR, or NR-loaded NSCLM, SCLM-50, and SCLM-100 micelles at equivalent NR concentrations (1, 5, 10, and 100 nM) for 2 h. Treated PC-3 and C4-2B cells were washed three times with PBS before being trypsinized with 0.05% trypsin−EDTA solution, centrifuged at 1000 rpm for 5 min to form pellets, suspended in 1 mL of PBS, and analyzed using CyAn ADP Flow Analyzer (Beckman Coulter, Brea, CA) at characteristic NR excitation (λ_{ex} = 488 nm) and emission (λ_{em} = 617 nm) wavelengths.

We investigated the effect of NSCLM, SCLM-50, and SCLM-100 micelles on the fluidity of PC-3 and C4-2B cell membranes using the 1,6-diphenyl-1,3,5-hexatriene (DPH) probe following published protocols.[41] Briefly, suspensions of PC-3 and C4-2B were washed twice with PBS before incubating with 2 μM DPH staining solution for 1 h at 37 °C. Cells were pelleted down and washed twice with PBS to remove excess DPH before suspending them in PBS and mixing with different micelle solutions at a micelle concentration of 1 nM.[42] We measured the fluorescence intensity of DPH (λ_{ex} = 365 nm and λ_{em} = 400−500 nm) directly before adding the micelle solution and at different incubation time points up to 1 h using a QM4 fluorescence spectrophotometer (PerkinElmer, Waltham, MA). Using DPH fluorescence at different time points, we calculated the change in membrane microviscosity using the following equation.

$$r_o/r = 1 + C(r)T\tau/\eta \quad (3)$$

where r_o is the limiting fluorescence anisotropy for DPH, which equals 0.362, and r is the measured fluorescence anisotropy at different time points. T is the absolute temperature, τ is the exited state lifetime that equals 10 ns, and $C(r)$ is a molecular shape parameter, which equals 8.6×10^5 poise·deg^{-1}·s^{-1}.[41] Membrane microviscosity was normalized to its intrinsic (baseline) viscosity observed before incubating with different micelles to show the change in membrane fluidity in response to different micelles as a function of incubation time.

2.10. Anticancer Activity of CTX-Loaded Micelles. PC-3 and C4-2B cells were seeded at a seeding density of 10×10^3 cells/well in 96-well plates and allowed to adhere for 24 h before incubating with free CTX and CTX-loaded NSCLM, SCLM-50, and SCLM-100 micelles at equivalent concentrations (500, 200, 100, 75, 50, 25, 10, 7.5, 5, 2.5, 1, 0.5, and 0.1 nM) of CTX for 48 h. PC-3 and C4-2B cells were also incubated with empty NSCLM, SCLM-50, and SCLM-100 micelles at the same amounts used to deliver different doses of CTX to assess the intrinsic toxicity of the micelles. At the end of the incubation period, the culture medium was aspirated and cells were incubated with 200 μL of the Resazurin dye at a dilution of 1/10 for 3 h before measuring solution fluorescence (λ_{ex} = 570 nm, λ_{em} = 590 nm) using the Fluoroskan Ascent FL plate reader. Fluorescence values were normalized to that observed with PC-3 and C4-2B cells incubated in the regular culture medium (control group) to calculate the percentage of viable cells in response to different treatments.

2.11. Intrinsic Micelle Toxicity. We evaluated the micelles' toxicity on normal healthy cells by incubating HEK 293 cells with empty NSCLM and SCLM-50 micelles. Briefly, HEK 293 cells were seeded at a seeding density of 10,000 cells/well in 96-well plates and allowed to adhere overnight before incubating with empty (no CTX loading) NSCLM and SCLM-50 micelles for 48 h. We measured the change in the proliferation of HEK 293 cells incubated with increasing concentrations of NSCLM and SCLM-50 micelles reaching 50−100-fold the IC_{50} of CTX when delivered using the same carriers compared to untreated HEK 293 cells (control). Change in cell proliferation was quantified by aspirating the particle solution and incubating the cells with 200 μL of the Resazurin dye at a dilution of 1/10 for 4 h before measuring solution fluorescence (λ_{ex} = 570 nm, λ_{em} = 590 nm) using the Fluoroskan Ascent FL plate reader. Fluorescence values were normalized to that of untreated HEK 293 cells (control group) to calculate the percentage of viable cells in response to different concentrations of NSCLM and SCLM-50 micelles.

2.12. Hemocompatibility Assays. We evaluated the hemocompatibility of NSCLM, SCLM-50, and SCLM-100 micelles by investigating the adsorption of bovine serum albumin (BSA) as a model serum protein to the micelle surface as a function of time and micelle interaction with red blood cells (RBCs) and platelets *in vitro*.

Briefly, blood samples were freshly collected from human volunteers following IRB-approved protocols into 10 mL of EDTA-coated Vacutainer tubes before centrifuging at 3,000 rpm for 5 min to separate the RBCs from the plasma supernatant. The RBC layer was washed three times with 0.15 M sodium chloride solution before diluting to a total volume of 10 mL using PBS (pH 7.4) by gently inverting the tube

DOI: 10.1021/acs.molpharmaceut.6b00147
Mol. Pharmaceutics 2016, 13, 1413−1429

following published protocols.[43] Approximately 2.5×10^7 RBCs were mixed with 550 μL of PBS (pH 7.4) and 250 μL of 1 μM NSCLM, SCLM-50, or SCLM-100 solutions in Eppendorf tubes that were incubated in a shaking water bath at 37 °C for 1 h. All tubes were centrifuged at 14000*g* for 5 min to pellet down the RBCs, and 200 μL of the supernatant solutions was transferred into a flat-bottom 96-well plate to measure the UV absorbance of the leaked hemoglobin at 541 nm using the Multiskan microplate reader (Thermo Fisher Scientific Inc., Waltham, MA). Absorbance of each supernatant solution was normalized to the UV absorbance of the supernatant solution of RBCs incubated with Triton X-100 (positive control) to calculate % RBCs hemolysis triggered by incubation with different micelle formulations.

To investigate platelet interaction with different micelles, we collected fresh blood from euthanized C57BL/6 mice using 20 gauge needles flushed with 3.2% sodium citrate, which was mixed with 1 volume of HEPES Tyrode buffer before centrifuging twice at 50*g* for 10 min to collect the platelet rich plasma (PRP) layer. The blood was centrifuged one more time with 1 volume of HEPES tyrode buffer at 1200*g* to collect the platelet poor plasma (PPP) layer. We mixed 10 μL of 1 μM NSCLM, SCLM-50, and SCLM-100 solutions with 500 μL of PRP solution prewarmed to 37 °C followed by monitoring platelet aggregation over a period of 10 min using the Aggro-Link data reduction system (Chrono-log Corporation, Havertown, PA) following published protocols.[44−46] Similarly, we monitored platelet aggregation upon mixing 500 μL of PRP solution with 10 μL of 10 μM ADP and collagen (5 μM) (1:1 v/v) mixture and PBS as positive and negative controls, respectively.

Finally, we investigated binding of bovine serum albumin (BSA) as a model serum protein to SCLM-50 micelles (test) and G5-$(NH_2)_{128}$ dendrimers (positive control) to assess micelle opsonization as a function of incubation time. Briefly, SCLM-50 micelles and G5-$(NH_2)_{128}$ particles were dissolved in PBS (pH 7.4) at a 250 nM particle concentration, mixed with BSA solution (0.5 mg/mL) in a quartz cuvette, and incubated at 37 °C for 60 min. We measured the fluorescence of BSA tryptophan residues (λ_{ex} = 280 nm, λ_{em} = 300−400 nm) at time zero ($I°$) and at different incubation time points (I) using the QM4 fluorescence spectrophotometer (PerkinElmer, Waltham, MA). We quantified the quenching of BSA fluorescence as a function of incubation time by dividing initial BSA fluorescence ($I°$) by that observed at different time points (I). We compared the calculated $I°/I$ ratio for BSA incubated with different particle solutions to that of BSA alone at different time points using Student's *t* test to determine the statistical significance in the observed change in BSA fluorescence at different time points.

2.13. Macrophage Uptake of Opsonized Micelles. We investigated the phagocytosis of NSCLM, SCLM-50, and SCLM-100 micelles by differentiated THP-1 (dTHP-1) cells to determine their ability to resist opsonization and clearance by activated macrophages. Briefly, NR-loaded NSCLM, SCLM-50, and SCLM-100 were dissolved in PBS at a NR concentration of 10 nM before mixing with 4 mL of fetal bovine serum (FBS) and incubating for 1 h at 37 °C to allow micelle opsonization by serum proteins. The opsonized particles were then incubated in regular culture medium with dTHP-1 cells for 2 h at 37 °C followed by aspirating the culture medium, washing the cells with PBS, and treatment with Accutase to detach the THP-1 cells forming a cell suspension. THP-1 cell suspensions were centrifuged at 1,000 rpm for 5 min and suspended in PBS before being analyzed by flow cytometry using CyAn ADP Analyzer to determine the number of NR- labeled cells. Uptake of FITC-IgG (Phagocytosis Assay Kit, Cayman Chemical, Ann Arbor, MI) by dTHP-1 cells was quantified following manufacturer's protocol. Uptake of different particles into dTHP-1 cells was normalized to that of FITC-IgG (positive control) to determine the ability of different particles to resist opsonization by serum proteins and phagocytosis by activated macrophages.

3. RESULTS AND DISCUSSION

3.1. Synthesis of Amphiphilic PMMA-*b*-PAA-*b*-PEG Polymer. It is critical to achieve control over the size/molecular weight of the hydrophilic and hydrophobic blocks to trigger the assembly of narrowly dispersed micelles. Therefore, we utilized a combination of ATRP technique and alkyne−azide cycloaddition "*click*" reaction to synthesize the amphiphilic PMMA-*b*-PAA-*b*-PEG polymer with a well-defined composition and molecular weight. The literature provides multiple examples of the ability to inhibit nonspecific adsorption of serum proteins to particle surface and the associated clearance by phagocytic macrophages using a "brush" of PEG chains with an average molecular weight of 5 kDa.[47] Therefore, we decided to use a 5 kDA PEG block in the synthesis of the PMMA-*b*-PAA-*b*-PEG polymer. Given FDA approval of using PMMA, P*t*BA, and PAA polymers as excipients in controlled-release pharmaceutical formulations,[48−50] we similarly used MMA and *t*BA monomers to synthesize the hydrophobic PMMA block and central PAA block, respectively. To achieve hydrophilic/hydrophobic balance in polymer composition, the target molecular weight of the hydrophobic block was 5 kDa. By adjusting the molar feed ratio of the MMA monomer, the ethyl-2-bromoisobutyrate initiator, and PMDETA ligand to 200/1/1 and allowing the polymerization reaction to go for 21 min at 40 °C, we were able to synthesize the PMMA block with the desired molecular weight. Calculating the ratio between the methyl protons of the MMA monomers appearing at 3.57 ppm to the initiator protons at 4.21 ppm shows the polymerization of 44 MMA units forming the PMMA block with a M_{nNMR} of 4603 g/mol (Figure S1). GPC analysis of the PMMA block shows a symmetric unimodal peak indicating a M_{nGPC} of 4855 g/mol and a polydispersity index (PDI, M_w/M_n) of 1.27 (Figure S9). Both ^{1}H NMR and GPC analysis confirm successful synthesis of the PMMA block with the desired molecular weight.

We used PMMA-Br as a macroinitiator to start the polymerization of *t*BA monomers with the goal of extending the PMMA block with 25 units of *t*BA monomers. By adjusting the ratio of *t*BA monomers, PMMA-Br as a macroinitiator, and PMDETA ligand to 100/1/1, 27 *t*BA monomers were polymerized into the P*t*BA block with M_{nNMR} of 8063 g/mol as shown in the ^{1}H NMR spectrum (Figure S2). GPC analysis of the PMMA-*b*-P*t*BA-Br copolymer shows a symmetric peak with an earlier elution volume indicating a M_{nGPC} of 9596 g/mol and a PDI (M_w/M_n) of 1.23. The terminal Br groups transformed to azide were monitored by ^{1}H NMR (Figure S3) and FT-IR. Similarly, our results show that commercial PEG was reacted with 4-pentynoic acid, and results show that ≥95% of the terminal OH groups were converted to alkynes (Figure S4). PEG-alkyne and PMMA-*b*-P*t*BA-N_3 were "*clicked*" with a 95% efficiency to form the PMMA-*b*-P*t*BA-*b*-PEG polymer, which is confirmed by the characteristic proton of the triazole

DOI: 10.1021/acs.molpharmaceut.6b00147
Mol. Pharmaceutics 2016, 13, 1413−1429

ring at 7.46 ppm (Figure S5) and loss of the azide and alkyne peaks on the FTIR spectrum. The ^{1}H NMR spectrum of PMMA-*b*-P*t*BA-*b*-PEG polymer shows a M_{nNMR} of 11 547 g/mol while GPC analysis shows a M_{nGPC} of 14 860 g/mol and a PDI (M_w/M_n) of 1.15. We decided to polymerize *t*BA monomers instead of AA monomers to avoid the reported reaction of the carboxylic acid groups with the metal complexes, which interferes with ATRP.[51] We removed the *tert*-butyl groups by acid-mediated hydrolysis using TFA, which is confirmed by the disappearance of the methyl protons of the *tert*-butyl groups at 1.43 ppm (Figure S6).

3.2. Micelle Formulation and Characterization. Similar to other amphiphilic polymers,[52,53] we expected PMMA-*b*-PAA-*b*-PEG polymer to self-assemble into micelles with the PMMA block forming the hydrophobic core, the PAA block forming a hydrophilic shell, and the PEG block forming an extended brush when added to aqueous solutions. To determine the critical micelle concentration (CMC) of PMMA-*b*-PAA-*b*-PEG polymer, we monitored the change in the intensity of NR fluorescence upon increasing polymer concentration in water. Specifically, we relied on monitoring the increase in NR fluorescence upon transitioning from the bulk aqueous solution to the hydrophobic environment within the micelle's core to determine whether the polymer exists in a unimer or micelle conformation similar to previous reports.[54,55] Results show baseline NR fluorescence in the presence of low concentrations (0.1−10 μg/mL) of PMMA-*b*-PAA-*b*-PEG polymer, which gradually increased with the increase in polymer concentration above 11 μg/mL (Figure 2). This

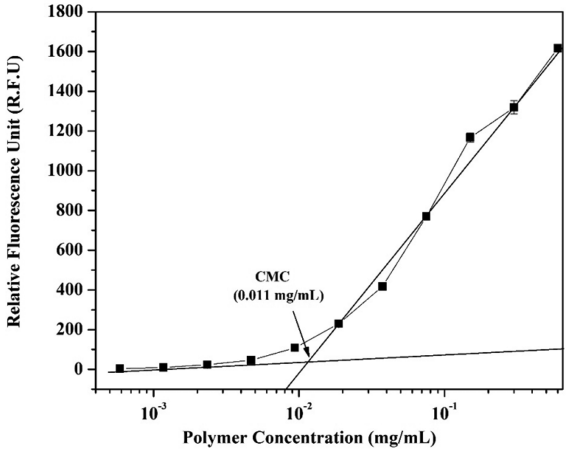

Figure 2. Relationship between the concentration of PEG-*b*-PAA-*b*-PMMA polymer and NR fluorescence, which is used to calculate the critical micelle concentration (CMC).

change in NR fluorescence as a function of polymer concentration shows that the PMMA-*b*-PAA-*b*-PEG polymer switches from a unimer to a self-assembled micelle at a critical micelle concentration (CMC) of 11 μg/mL (Figure 2). Given that the literature shows CMC values ranging between 0.3 and 70 μg/mL for different polymer compositions,[56−61] the observed low CMC for PMMA-*b*-PAA-*b*-PEG polymer indicates the stability of the formed micelles and their potential as drug delivery vehicles.

One of the key challenges with self-assembled carriers including micelles is their dilution when injected into the systemic circulation, which brings polymer concentration below the CMC causing rapid release of the loaded cargo before reaching the targeted tissue.[62] For micelles loaded with chemotherapeutic agents, the "burst" release of the loaded cargo results in significant systemic toxicity,[63] which dramatically reduces their clinical value. To address this issue, we designed an acid-labile linker with two terminal amine (NH_2) groups, which can react with the carboxylic acid groups (COOH) in the central PAA block to cross-link or "stitch" adjacent polymer chains forming an acid-sensitive shell. We hypothesized that SCLM will retain the loaded drug better than NSCLM and will selectively release their cargo when internalized via endocytosis into cancer cells in response to the acidic pH of the endosomes.

Both ^{1}H NMR and ^{13}C NMR analysis were used to confirm shell cross-linkage in SCLM compared to NSCLM (Figure 3). Figure 3A shows the ^{1}H NMR spectrum of the diamine cross-linker and the four characteristic H_a−H_d proton peaks. Specifically, the protons (H_a) of the two geminal methyl groups are observed as a singlet at δ 1.36 ppm, the two CH_2 protons (H_b) next to the oxygen atoms are observed as a triplet at δ 3.45 ppm, the two CH_2 protons (H_c) next to the amines are observed as a multiplet at δ 2.81 ppm, and the amine protons (H_d) are observed as a broad singlet at δ 1.44 ppm. By comparing the ^{1}H NMR spectra of SCLM and NSCLM (Figure 3B), one can identify the characteristic proton peaks of the linker in SCLM spectrum, which confirms successful cross-linkage of the polymer shell. Briefly, the protons (H_a) of the two geminal methyl groups are observed as a triplet at δ 0.96 ppm with a coupling constant <1.0 Hz, which indicates that H_a protons are tightly packed close to the H_b protons. Similarly, H_b and H_c protons are observed as multiplets at δ 3.33 ppm and δ 3.05 ppm while the amine proton (H_d) is observed at δ 7.66 ppm indicating the formation of amide bonds confirming shell cross-linkage. The ^{13}C NMR spectra of the diamine cross-linker, SCLM, and NSCLM provide additional evidence of successful shell cross-linkage in SCLM. Specifically, the ^{13}C NMR spectrum of the diamine linker in $CDCl_3$ shows the two geminal CH_3 (C_a) at δ 24.98 ppm and the peaks of C_b and C_c carbons at δ 62.88 ppm and δ 42.18 ppm, respectively, while the quaternary carbon (C_d) peak is observed at δ 99.79 ppm (Figure 3C). Similarly, the ^{13}C NMR of SCLM shows C_a, C_b, and C_c peaks at δ 23.54, δ 62.15, and δ 51.05 ppm (Figure 3D), which corresponds to their characteristic shifts observed in the cross-linker spectrum. It is important to note that the characteristic cross-linker peaks are missing in the ^{1}H NMR and ^{13}C NMR spectra of NSCLM, confirming successful cross-linkage of the polymer shell in SCLM only.

We characterized the size and surface charge of empty (no cargo) and NR- and CTX-loaded micelles in NSCLM and SCLM using dynamic light scattering and zeta potential measurements, respectively. Results show that empty NSCLM and those loaded with NR and CTX have similar average sizes of 48.41 ± 3.92 nm, 42.88 ± 4.81 nm, and 46.68 ± 7.65 nm, respectively (Figure 4). Similarly, empty and NR- and CTX-loaded SCLM had average diameters of 46.44 ± 11.80 nm, 47.64 ± 15.48 nm, and 54.06 ± 9.14 nm, respectively. There was no statistical difference between empty and loaded micelles regardless of the type of cargo or whether the micelle shell was cross-linked or not, which indicates the stability of the formed micelles and their suitability to encapsulate a range of therapeutic molecules. Given that the gaps in the endothelial lining of tumor vasculature are 200−600 nm in size,[64] both NSCLM and SCLM can easily penetrate across leaky tumor vasculature and accumulate in tumor tissue *in vivo*. The

DOI: 10.1021/acs.molpharmaceut.6b00147
Mol. Pharmaceutics 2016, 13, 1413−1429

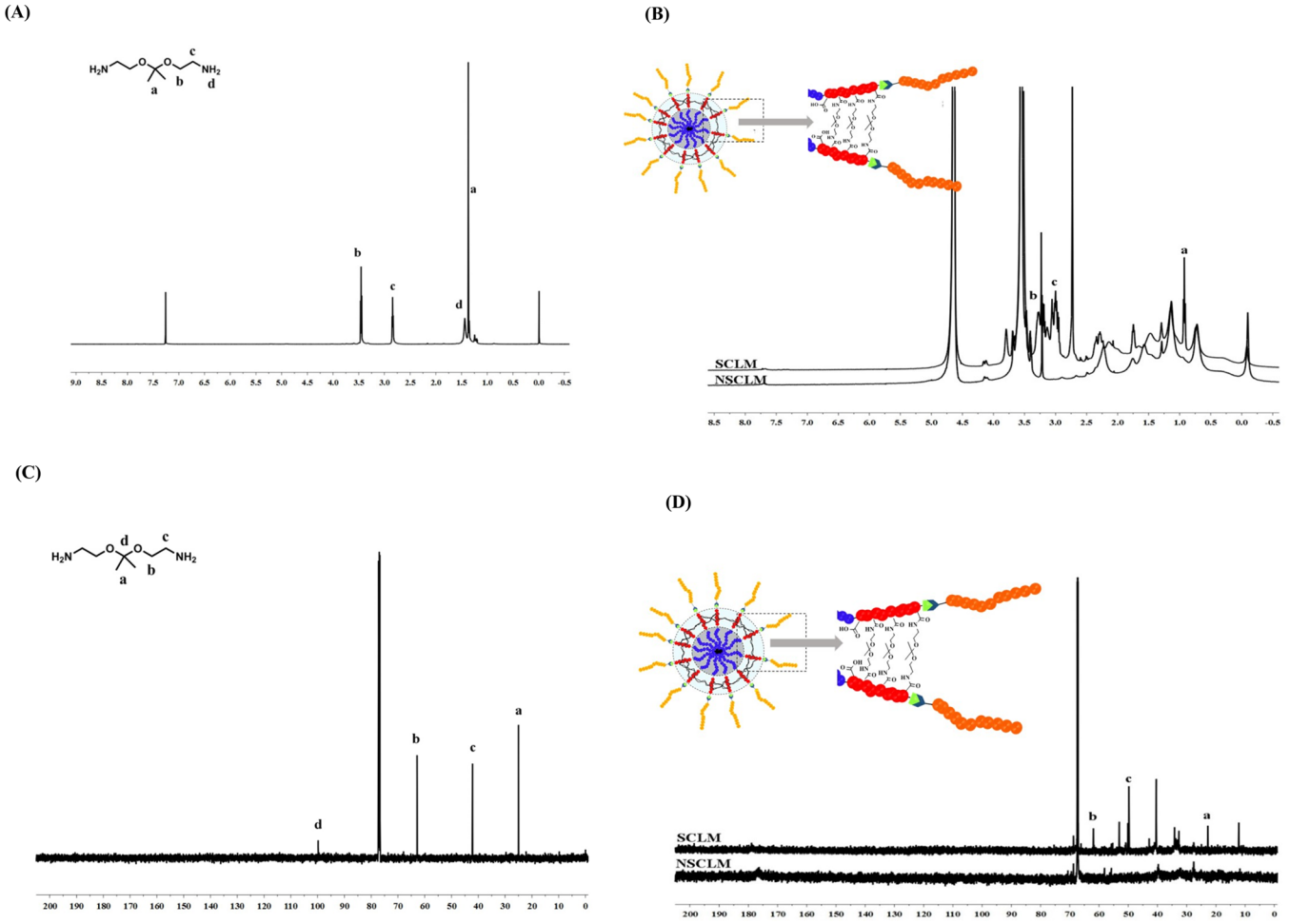

Figure 3. (A) ^{1}H NMR and (C) ^{13}C NMR of the acid-labile 2,2′-(propane-2,2-diylbis(oxy))-diethanamine cross-linker recorded in $CDCl_3$. (B) ^{1}H NMR and (D) ^{13}C NMR of the NSCLM and SCLM micelles recorded in D_2O, which confirms successful cross-linkage of central PAA blocks.

recorded zeta potential of NSCLM and SCLM is −38.1 ± 3.16 mV and −24.5 ± 6.71 mV, respectively. The observed negative surface charge of the micelles is probably due to the free COOH groups in the central PAA block, which in combination with the PEG brush will minimize nonspecific interaction with serum proteins and the subsequent clearance by phagocytic macrophage cells (e.g., Kupffer cells in the liver).[47]

3.3. Nile Red and Cabazitaxel Release from NSCLM and SCLM. Release of drug molecules from the micelles' hydrophobic core is expected to change as a function of solution pH and incubation time. To test this hypothesis, we evaluated the release of NR as a model hydrophobic drug encapsulated in NSCLM, SCLM-50, and SCLM-100 in PBS (pH 7.4) and citrate buffer (pH 5.0) to predict NR release in the systemic circulation and the acidic endosomes, respectively. Results show that encapsulation efficiency of NR in NSCLM, SCLM-50, and SCLM-100 micelles was 82.29 ± 7.53%, 71.64 ± 6.61%, and 81.15 ± 7.32%, respectively. We aimed to achieve 10% w/w loading of NR in different micelles, and results show 7.60 ± 0.64%, 6.69 ± 0.38%, and 7.51 ± 0.59% w/w loading in NSCLM, SCLM-50, and SCLM-100 micelles, respectively. Using micelle solutions containing 0.5 mg/mL polymer (i.e., ∼50-fold the CMC) and encapsulating NR loaded in dialysis bags with MWCO 3500 Da, we investigated NR release in different buffer solutions by measuring NR fluorescence (λ_{ex} = 550 nm and λ_{em} = 620 nm) at different time points up to 30 h.

Results show that 0.52 ± 0.14% of the loaded NR was released from NSCLM after 3 h in PBS (pH 7.4) and gradually increased with the increase in incubation time reaching 43.59 ± 1.38% of the loaded NR after 30 h (Figure 5A). In comparison, 0.26 ± 0.11% of the loaded NR was released after 3 h of dialyzing SCLM-100 micelles against PBS (pH 7.4), which gradually increased, reaching 28.35 ± 0.88% of the loaded NR after 30 h. The observed decline in cumulative NR release from SCLM-100 compared to NSCLM clearly indicates that cross-linkage of the carboxylic acid groups in the central PAA block significantly reduces "burst" release of the loaded cargo at physiologic pH. Reducing the number of cross-linked carboxylic acid groups by 50% in SCLM-50 resulted in release of 0.3 ± 0.08% of the loaded NR over 3 h, which gradually increased, reaching 45.20 ± 0.93% of the loaded NR after 30 h. Comparing NR release profiles from SCLM-50 and SCLM-100 shows that controlling the degree of cross-linkage of carboxylic acid groups in the central PAA block controls the release of the encapsulated cargo in physiologic pH.

By changing the dialysis solution to citrate buffer, we investigated the release of the encapsulated NR in acidic environment (pH 5.0) similar to that of the endosomes. Results show that 0.06 ± 0.03% of the loaded NR in NSCLM was released over 1.5 h and gradually increased reaching 90.93 ± 1.36% of the loaded cargo over 30 h (Figure 5A). In comparison, 0.68 ± 0.22% of the loaded NR in SCLM-100

DOI: 10.1021/acs.molpharmaceut.6b00147
Mol. Pharmaceutics 2016, 13, 1413−1429

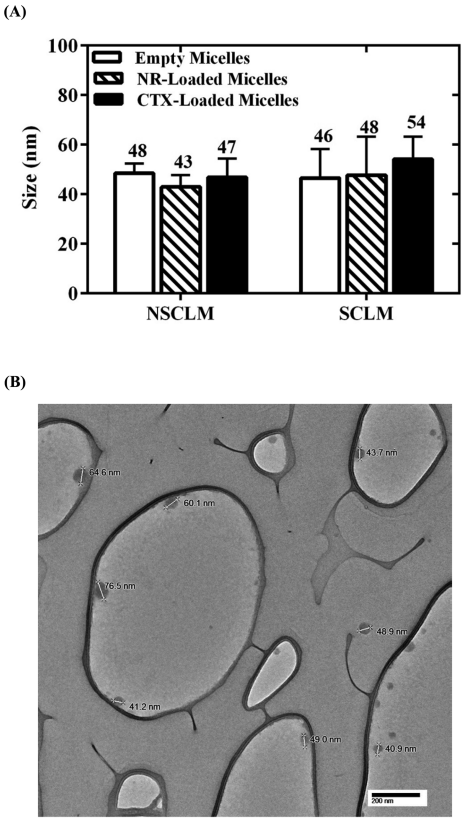

Figure 4. (A) The size of empty, NR-loaded, and CTX-loaded micelles. Results show the average + standard error of the mean (SEM) of three independent solutions for each micelle formulation. (B) Transmission electron microscopy (TEM) image showing the shape and size of NSCLM micelles.

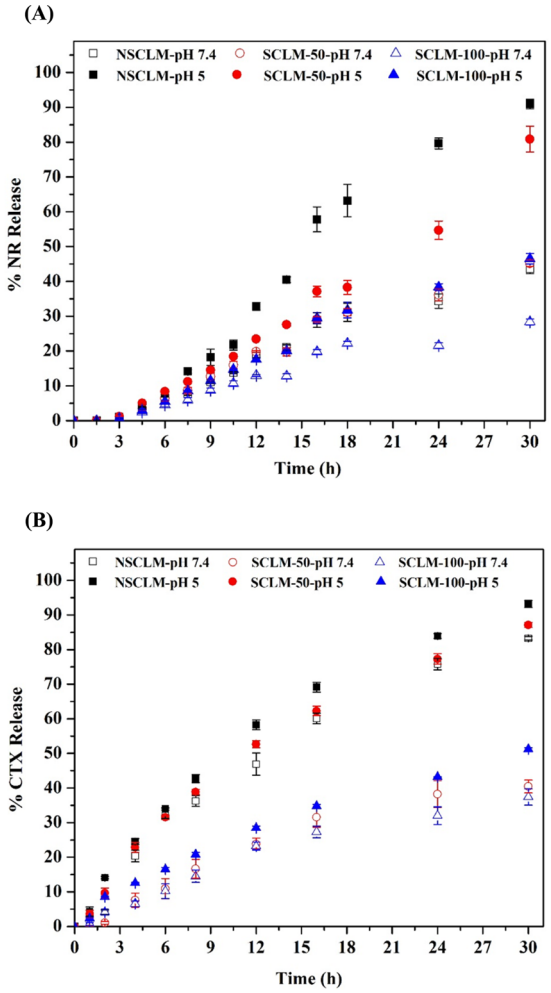

Figure 5. Release of NR (A) and CTX (B) from NSCLM, SCLM-50, and SCLM-100 micelles in PBS (pH 7.4) and acetate buffer (pH 5.0) solutions as a function of time.

micelles was released over 3 h and increased reaching 46.52 ± 1.49% over 30 h, which is significantly higher ($p \leq 0.001$) than NR release observed in neutral PBS (pH 7.4). Similarly, 1.18 ± 0.16% of the loaded NR in SCLM-50 micelles was released over 3 h and increased reaching 80.89 ± 3.69% over 30 h, which is significantly higher ($p \leq 0.001$) than NR released observed in neutral PBS (pH 7.4). Difference in NR release profiles from SCLM-50 and SCLM-100 in neutral (pH 7.4) and acidic (pH 5.0) buffers clearly confirms the sensitivity of the cross-linked polymer shell to the acidic stimuli as a release mechanism that still discriminates between different micelles based on their shell cross-linkage density.

Similarly, we prepared CTX-loaded NSCLM, SCLM-50, and SCLM-100 aiming to achieve 10% w/w loading of CTX, and results show w/w loading of 5.18 ± 0.53%, 3.77 ± 0.36%, and 4.72 ± 0.04%, respectively. Results also show that encapsulation efficiency of CTX in NSCLM, SCLM-50, and SCLM-100 micelles was 54.63 ± 5.94%, 39.13 ± 3.89%, and 49.58 ± 0.41%, respectively. Size of CTX-loaded NSCLM and SCLM-100 particles was 46.68 ± 7.65 nm and 54.06 ± 9.14 nm, which is similar to the size of empty and NR-loaded micelles (Figure 4). We quantified CTX release from CTX-loaded NSCLM, SCLM-50, and SCLM-100 micelle solutions loaded in dialysis bags with MWCO 3500 Da and placed in PBS (pH 7.4) and citrate buffer (pH 5.0) at different time points up to 30 h. As expected, CTX was quickly released from NSCLM in PBS buffer (pH 7.4) starting with 4.12 ± 0.63% within 2 h and gradually increasing to reach 83.21 ± 0.52% of the loaded cargo after 30 h (Figure 5B). CTX release from NSCLM into citrate buffer (pH 5.0) started with 14.11 ± 0.34% of the cargo within 1 h and gradually increased reaching 93.16 ± 1.01% over 30 h (Figure 5B). In comparison, CTX release from SCLM-100 micelles in PBS buffer (pH 7.4) started with 4.1 ± 0.83% over 2 h and gradually increased to 37.43 ± 2.35% over 30 h (Figure 5B), which is a lower cumulative release than that observed with NSCLM due to cross-linkage of 100% of the central acrylic acid groups. In citrate buffer (pH 5.0), CTX release started at 8.56 ± 0.22% over 2 h and increased to 51.26 ± 0.39% over 30 h due to hydrolysis of the acid-labile linker and release of the encapsulated cargo (Figure 5B). SCLM-50 micelles released 1.09 ± 0.41% of the loaded CTX over 2 h in PBS buffer (pH 7.4) which increased to 40.45 ± 1.83% over 30 h, which is a similar release profile to that observed with SCLM-100 micelles in neutral pH. However, 9.68 ± 1.40% of the loaded CTX was released over 2 h in citrate buffer (pH 5.0) and increased to 87.13 ± 0.71% over 30 h (Figure 5B). This higher CTX release in acidic citrate buffer is a result of cross-linkage of only 50% of the central acrylic acid groups. These results collectively indicate successful formulation of acid-sensitive SCLM that efficiently encapsulated CTX and retained the bulk of the loaded cargo at physiologic pH but quickly released it in response to acidic stimuli similar to those established in the endosome.

DOI: 10.1021/acs.molpharmaceut.6b00147
Mol. Pharmaceutics 2016, 13, 1413−1429

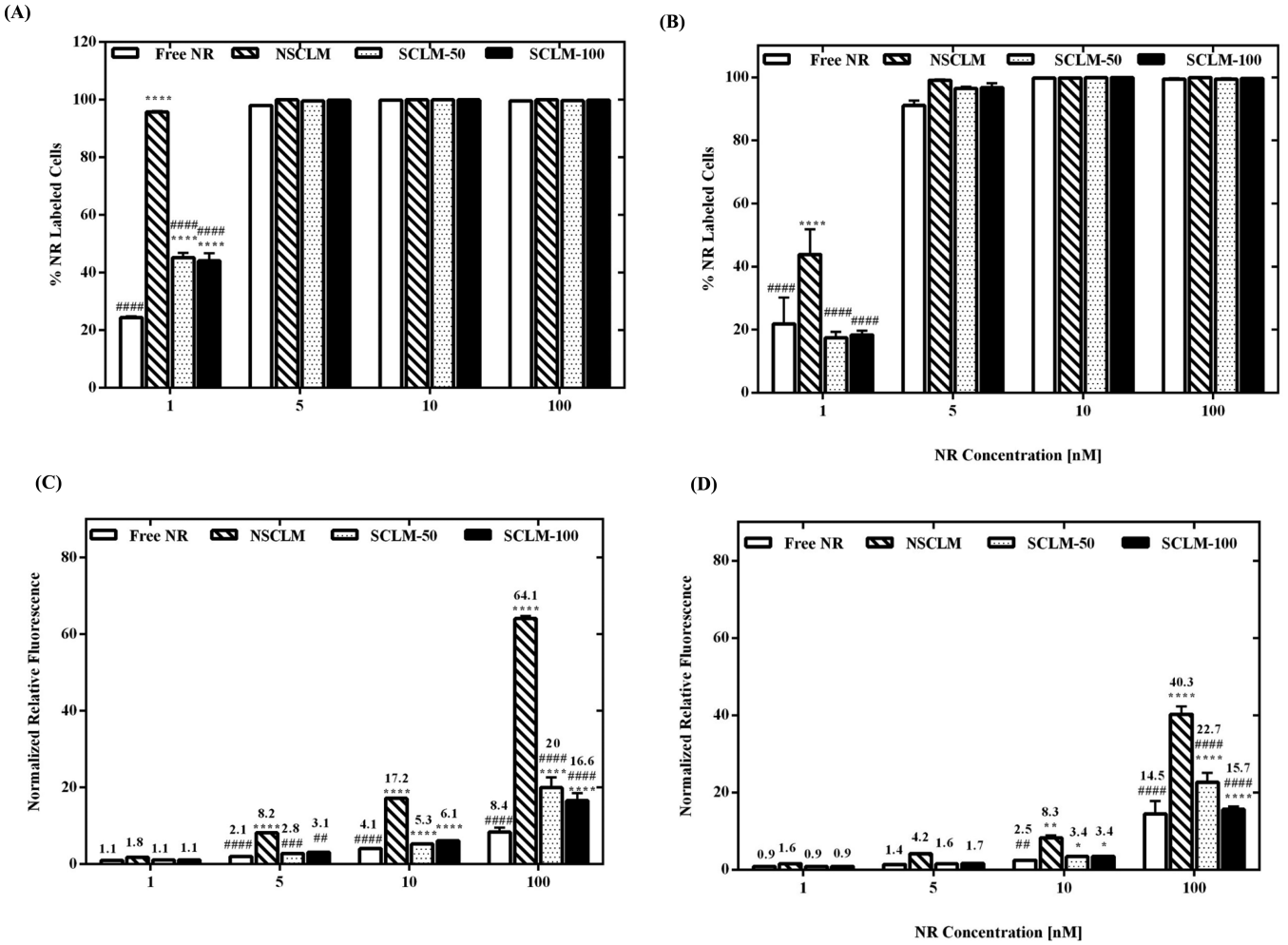

Figure 6. Uptake of free NR and NR-loaded NSCLM, SCLM-50, and SCLM-100 micelles into PC-3 (A, C) and C4-2B (B, D) prostate cancer cells. Results are the average of four samples + standard error of the mean. Statistical difference between the uptake of SCLM-50 and SCLM-100 micelles and the uptake of free NR (*) and NSCLM (#) was evaluated using two-way ANOVA with Tukey's multiple comparisons test where * and # denote $P \leq 0.05$, ** and ## denote $P \leq 0.01$, *** and ### denote $P \leq 0.001$, and **** and #### denote $P \leq 0.0005$.

3.4. Cell Uptake of NR-Loaded Micelles. We investigated the uptake of NR-loaded NSCLM, SCLM-50, and SCLM-100 micelles compared to free NR into PC-3 and C4-2B cells after incubating for 2 h at 37 °C by measuring the percentage of NR-labeled cells and the intensity of NR fluorescence per cell as a function of NR concentration (1, 5, 10, 100 nM) using flow cytometry. Results show that NR-loading into NSCLM, SCLM-50, and SCLM-100 micelles labeled 95.74 ± 0.27%, 45.23 ± 1.61%, and 44.11 ± 2.64% of PC-3 cells, which is significantly higher than the 24.35 ± 0.56% cells labeled by free NR at NR concentration of 1 nM (Figure 6A). At higher NR concentrations, 100% of PC-3 cells were labeled upon incubation with free NR and NR-loaded micelles. However, by analyzing the intensity of intracellular fluorescence at each concentration of NR, results show that NR loading into NSCLM, SCLM-50, and SCLM-100 micelles significantly increased the amount of NR delivered into the cytoplasm of each cell compared to free NR at 5, 10, and 100 nM (Figure 6C).

Incubating C4-2B cells with 1 nM NR loaded into NSCLM, SCLM-50, and SCLM-100 micelles results in labeling 43.84 ± 7.97%, 17.37 ± 1.91%, and 18.32 ± 1.31% of the cells compared to labeling 21.81 ± 8.43% of the cells by the free NR (Figure 6B). At higher NR concentrations (5, 10, and 100 nM), 100% of PC-3 cells were labeled upon incubation with free NR and NR-loaded micelles. However, analysis of the intensity of intracellular fluorescence at each concentration shows that NSCLM exhibits higher intracellular fluorescence at a low concentration of 5 nM compared to free NR (Figure 6D), whereas SCLM-50 and SCLM-100 micelles exhibited higher intracellular fluorescence compared to free NR only at the concentration of 100 nM (Figure 6D).

The observed increase in intracellular fluorescence of PC-3 and C4-2B cancer cells upon incubation with NR-loaded NSCLM compared to free NR and NR-loaded SCLM-50 and SCLM-100 micelles (Figure 6C,D) is an interesting observation that prompted further investigation. We hypothesized that dilution of the NSCLM solution in the culture medium led to release of PEG-*b*-PAA-*b*-PMMA unimers that insert the hydrophobic PMMA block into the cell membrane causing an increase in membrane fluidity, which enhances the diffusion of NR into the cells. To test this hypothesis, we investigated the interaction between NSCLM and SCLM-100 micelles with PC-3 and C4-2B cells based on the change in the fluorescence polarization spectrum of DPH compared to untreated (control) cells following published methods.[42,65,66] Results show that PC-3 and C4-2B cells treated with NSCLM at the concentration needed to deliver 1 nM NR show a rapid drop in membrane

DOI: 10.1021/acs.molpharmaceut.6b00147
Mol. Pharmaceutics 2016, 13, 1413−1429

microviscosity within 15 min, which remained constant for 60 min (Figure 7A,B). In comparison, cells treated with SCLM-

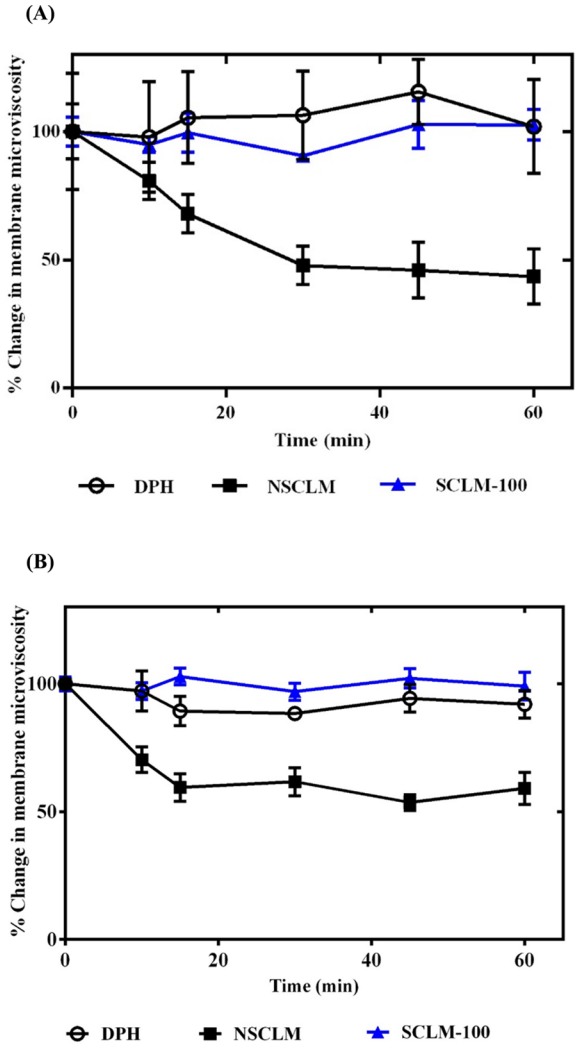

Figure 7. Change in microviscosity of the membranes of PC-3 (A) and C4-2B (B) prostate cancer cells indicated by the drop in DPH fluorescence as a function of incubation time with NSCLM and SCLM-100 micelles. Results show the average of the calculated microviscosity at different time points normalized to its initial value (time = 0 min, 1.40 ± 0.22 poise for PC-3 cells and 24.43 ± 0.52 poise for C4-2B cells) ± standard error of the mean.

100 micelles did not exhibit any change in membrane microviscosity, which was similar to that observed with control cells (i.e., treated with DPH only) (Figure 7A,B). These results are supported by previous reports showing that P85 block copolymer increases the fluidity of the cell membrane when used at concentrations lower than the critical micelle concentration (CMC) due to interaction of the hydrophobic poly(propylene oxide) block with the lipid bilayer.[67]

3.5. Cytotoxicity of CTX-Loaded Micelles. We compared the effect of free CTX and CTX-loaded NSCLM, SCLM-50, SCLM-100 micelles on the viability of PC-3 and C4-2B prostate cancer cells as a function of CTX concentration (0.1−500 nM). Results also show that NSCLM and SCLM-50 micelles exhibit higher toxicity toward PC-3 (Figure 8A) and C4-2B cells (Figure 8B) compared to equal concentrations of free CTX. The difference in cytotoxicity of different micelles

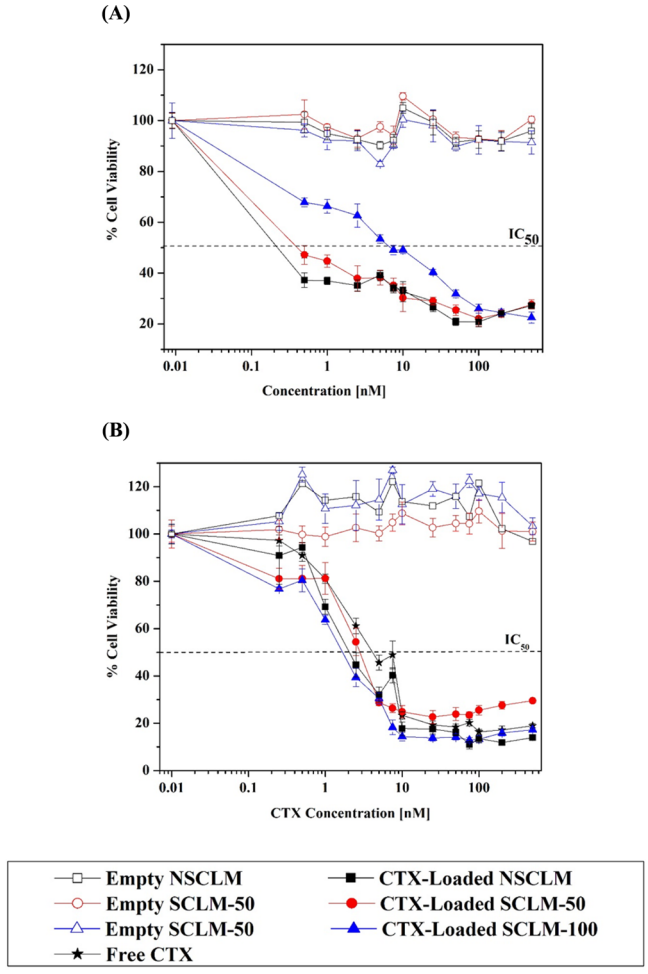

Figure 8. Effect of free CTX, CTX-loaded micelles, and empty micelles on PC-3 (A) and C4-2B (B) prostate cancer cells as a function of equivalent CTX concentration (0.01−500 nM). Each experiment was carried out in triplicate. Results represent the average ± standard error of the mean. Curves were fitted to a log concentration versus % surviving fraction (% SF) model using GraphPad Prism Software. The IC_{50} value for each treatment (dotted horizontal line) was calculated using GraphPad Prism Software.

compared to free CTX is indicated by the difference in their IC_{50} values (Figure 8 and Table 1). Results show IC_{50} for CTX-

Table 1. IC_{50} of Free CTX and CTX-Loaded Micelles in PC-3 and C4-2B Cells

	IC_{50} (nM)	
treatment	in PC-3 cells	in C4-2B cells
free CTX	0.96 ± 0.20	3.33 ± 0.63
CTX-loaded NSCLM	0.60 ± 0.17	2.66 ± 0.81
CTX-loaded SCLM-50	0.76 ± 0.18	1.72 ± 0.52
CTX-loaded SCLM-100	5.08 ± 0.74	2.66 ± 0.56

loaded NSCLM and SCLM-50 micelles of 0.60 ± 0.17 and 0.76 ± 0.18 nM, respectively, which is significantly lower than the IC_{50} of free CTX (0.96 ± 0.20 nM) in PC-3 cells. Similarly, the IC_{50} of CTX-loaded NSCLM and SCLM-50 micelles (2.66 ± 0.81 and 1.72 ± 0.52 nM) in C4-2B cells is significantly lower than that of the free drug (3.33 ± 0.63 nM). The observed higher activity of CTX-loaded NSCLM and SCLM-50 micelles

DOI: 10.1021/acs.molpharmaceut.6b00147
Mol. Pharmaceutics 2016, 13, 1413−1429

can be attributed to higher uptake and efficient release of the cytotoxic cargo into cancer cells compared to the free drug.

It is interesting to note that SCLM-100 micelles are less toxic to cancer cells compared to NSCLM and SCLM-50 micelles despite their similar uptake, which is probably a result of the higher cross-linkage density of the central acrylic acid block resulting in slower or incomplete release of the encapsulated CTX cargo (Figure 8 and Table 1). Similarly, the observed higher toxicity of NSCLM and SCLM-50 micelles toward PC-3 cells compared to C4-2B can be attributed to a combination of factors including difference in intrinsic sensitivity toward CTX indicated by the lower IC_{50} of free CTX with PC-3 cells compared to C4-2B cells (Table 1). Further, the difference in the kinetics and net micelle uptake by both cells lines indicated by higher intracellular fluorescence observed with NR-loaded NSCLM and SCLM-50 micelles in PC-3 cells (Figure 6C) compared to C4-2B (Figure 6D) leading to a higher intracellular concentration of the toxic cargo in the cytoplasm of PC-3 compared to C4-2B resulting in higher cell death. The difference in micelle uptake between both cell lines has been reported and correlated with difference in the composition of the lipid membrane of both cell lines,[65,68] which further supports these results.

We also examined the effect of empty micelles (i.e., no CTX loading) on PC-3 and C4-2B cells' viability using the same micelle concentrations used to deliver a specific concentration of the toxic CTX cargo. Results show that empty NSCLM, SCLM-50, and SCLM-100 micelles did not negatively affect the viability of PC-3 and C4-2B cells (Figure 8). Furthermore, results also show no reduction in proliferation or viability of HEK 293 cells (a model of healthy organs) when incubated with NSCLM and SCLM-50 micelles at concentrations that are 50−100-fold higher than the IC_{50} of CTX delivered by these carriers (Figure 9). These results collectively indicate the biocompatibility of the polymeric carrier and the acid-labile linker used in micelle formulation.

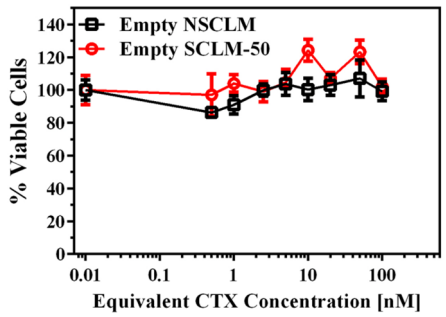

Figure 9. Effect of empty NSCLM and SCLM-50 micelles on HEK 293 cells as a function of micelle concentration used to deliver a given concentration of CTX (0.01−100 nM). Each experiment was carried out in triplicate. Results represent the average ± standard error of the mean.

3.6. Micelles' Hemocompatibility. *In vivo* activity of our micelles will depend on a delicate balance between their selective cytotoxicity toward prostate cancer cells while remaining inert toward healthy tissues and cells. The interaction between the micelles and serum proteins, red blood cells (RBCs), and macrophages in the blood influences micelles' residence in the systemic circulation, their clearance by the reticular endothelial system (RES), and their distribution profile.[69,70] Therefore, we investigated RBCs' hemolysis and platelet activation upon incubating with NSCLM, SCLM-50, and SCLM-100 micelles to determine their hemocompatibility. Results show that incubating NSCLM, SCLM-50, and SCLM-100 micelles needed to deliver 100 and 1000 nM CTX with RBCs caused hemolysis of only 3−4% of the cells, which is similar to the baseline hemolysis observed upon incubating RBCs with PBS (control) (Figure 10A). The lack of hemolytic

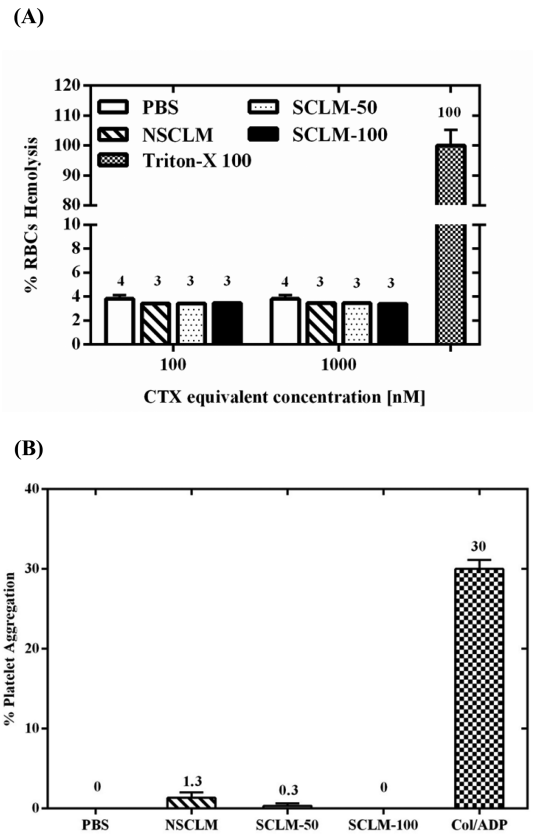

Figure 10. (A) The % of RBC hemolysis upon incubating with NSCLM, SCLM-50, and SCLM-100, normalized to that observed upon incubating the RBCs with Triton X-100 (positive control) for 60 min. RBCs were incubated with PBS (negative control) to determine baseline hemolysis due to cell handling. (B) The % of aggregated platelets observed upon incubation with PBS (negative control), NSCLM, SCLM-50, SCLM-100, and Col/ADP (positive control). Results show the average + standard error of the mean. The observed RBC hemolysis and platelet aggregation upon incubation with different micelle compositions was compared to that observed upon incubation with PBS two-way ANOVA with Tukey's multiple comparisons test.

capacity of our micelles at 50−500-fold the IC_{50} of CTX-loaded micelles is a result of high surface PEGylation, which has been shown to reduce the hemolytic activity of particulate carriers.[71]

Similarly, we investigated platelet activation when incubated with NSCLM, SCLM-50, and SCLM-100 micelles compared to collagen/ADP mixture (positive control) using light transmission aggregometry following published protocols.[46] Results show that SCLM-50 and SCLM-100 micelles caused insignificant platelet aggregation that was similar to that observed with PBS (negative control) (Figure 10B). However, NSCLM caused a slight increase in platelet aggregation compared to PBS, which can be attributed to the release of polymer unimers and exposure of the hydrophobic PMMA block that binds to and activate platelets in solution. These

DOI: 10.1021/acs.molpharmaceut.6b00147
Mol. Pharmaceutics 2016, 13, 1413−1429

results collectively indicate that SCLM-50 micelles are most suited for *in vivo* testing.

3.7. Micelles Opsonization and Macrophage Uptake. Adsorption of serum proteins to particulate carriers including micelles has been shown to be a key mediator of their recognition and clearance by the tissue-fixed macrophages including Kupffer cells in the liver plus splenic and lung macrophages.[70] Given that albumin is a major plasma protein,[72] we investigated its adsorption to micelle surface to determine the liability of different formulations to opsonization by serum proteins *in vivo*. We measured the change in the intrinsic fluorescence of the two tryptophan residues (λ_{ex} is 280 nm and λ_{em} is 300−400 nm) located in albumin's hydrophobic binding site to quantify albumin's adsorption to SCLM-50 micelles compared to G5-NH_2 (positive control) as a function of time following published protocols.[64] Results show that the fluorescence intensity of BSA mixed with SCLM-50 remained constant throughout the experiment with $I°/I \sim 1.1$, which is similar to the intrinsic fluorescence of free BSA (Figure 11A). In comparison, cationic G5-NH_2 particles strongly quenched BSA intrinsic fluorescence indicated by the difference in fluorescence intensity at the beginning of the study ($I°$) and at different time points (I) with more than 2-fold difference after 60 min. Results clearly show that the PEG corona of SCLM-50 coupled with the micelle neutral surface suppressed the albumin adsorption to the particle surface, which will dramatically reduce micelle clearance by the reticular endothelial system.

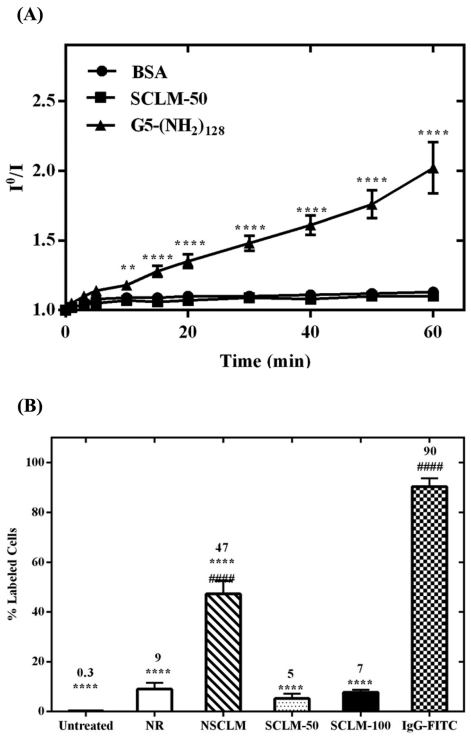

Figure 11. (A) The change in fluorescence intensity of BSA ($I°/I$) upon incubation of 0.2 mg/mL BSA with 250 nM cationic G5-$(NH_2)_{128}$ (positive control) and SCLM-50 particles (test) at 37 °C for 60 min. Results are the average of three samples ± standard error of the mean. Statistical difference between the fluorescence intensity of BSA ($I°/I$) upon incubation with different particles compared to that observed with free BSA at the same incubation time point is denoted by ** or ****, which indicates $p \leq 0.01$ or $p \leq 0.0005$, respectively. (B) Uptake of free NR, NR-loaded SCLM-50 and SCLM-100 micelles, and FITC-IgG (positive control) into differentiated THP-1 (dTHP-1) cells after incubating for 2 h at equivalent NR concentration of 10 nM. Results are the average of three samples + standard error of the mean. Uptake of NSCLM, SCLM-50, and SCLM-100 was compared to that of free NR (#) and FITC-IgG (*) using two-way ANOVA with Tukey's multiple comparisons test where * and # denote $P \leq 0.05$, ** and ## denote $P \leq 0.01$, *** and ### denote $P \leq 0.001$, and **** and #### denote $P \leq 0.0005$.

In order to investigate the effect of exposing different micelles to serum proteins on their recognition and internalization by tissue-resident macrophages, we evaluate the uptake of NR-loaded NSCLM, SCLM-50, and SCLM-100 micelles by differentiated THP-1 cells using flow cytometry. Specifically, we incubated 10 nM NR-loaded NSCLM, SCLM-50, and SCLM-100 micelles with fetal bovine serum (FBS) for 1 h at 37 °C to allow adsorption of a protein corona to the particle's surface before incubating with differentiated and activated dTHP-1 cells. Uptake of fluorescently labeled FITC-IgG was used to assess the phagocytic activity of dTHP-1 cells (i.e., positive control). Results show that FITC-IgG particles were internalized by 90% of dTHP-1 cells indicating strong activity of the phagocytosis machinery in these cells (Figure 11A). In comparison, SCLM-50 and SCLM-100 micelles were internalized by only 5% and 7% of dTHP-1 cells, which is similar to the uptake of free NR. This indicates the poor recognition of cross-linked micelles by activated macrophages even after exposure to serum proteins. In comparison, NSCLM labeled 50% of dTHP-1 cells indicating efficient delivery of the NR dye into the cells, which is not surprising given the similar effect observed with PC-3 and C4-2B cells (Figure 6) and the effect of polymer unimers on membrane fluidity (Figure 7). The observed higher uptake of 10 nM NR-loaded SCLM-50 and SCLM-100 by prostate cancer cells coupled with their significantly lower recognition and uptake by activated macrophages clearly indicates their ability to achieve selective delivery of their cargo to cancer cells while evading clearance by tissue-resident macrophages. Further, the optimized hydrolysis kinetics of the shell cross-linker in SCLM-50 coupled with efficient release of the loaded cargo makes this micelle composition particularly suited to be a platform for targeted delivery of anticancer drug into prostate cancer cells.

4. CONCLUSIONS

Results show the successful synthesis of an amphiphilic triblock copolymer (PMMA-*b*-PAA-*b*-PEG), which proved to self-assemble in aqueous media forming nanosized micelles that efficiently encapsulate hydrophobic small molecules like Nile Red and Cabazitaxel. Cross-linkage of the polymer shell using an acid-labile linker allows controlled and tunable release of the cytotoxic cargo. SCLM-50 micelles exhibited the highest cytotoxic activity toward PC-3 and C4-2B cancer cells *in vitro* with IC_{50} values that are significantly lower than that of free CTX. Further, SCLM-50 micelles did not cause hemolysis of RBCs, trigger platelet activation, acquire an albumin corona, or get phagocytosed by activated macrophages, which make this micelle platform an ideal carrier for selective delivery of CTX into prostate cancer cells.

■ ASSOCIATED CONTENT

Supporting Information

The Supporting Information is available free of charge on the ACS Publications website at DOI: 10.1021/acs.molpharmaceut.6b00147.

DOI: 10.1021/acs.molpharmaceut.6b00147
Mol. Pharmaceutics 2016, 13, 1413−1429

^{1}H NMR spectra and elution profiles on a size exclusion chromatography column (PDF)

AUTHOR INFORMATION

Corresponding Author

*University of Michigan, Department of Biomedical Engineering, 1101 Beal Avenue, 2150 Lurie Biomedical Engineering Building, Ann Arbor, MI 48109, USA. Phone: + 1 (734) 615-9404. E-mail: melsayed@umich.edu. Web: www.bme.umich.edu/centlab.php.

Author Contributions

‡O.A. and I.Y. contributed equally to this research work

Notes

The authors declare no competing financial interest.

ACKNOWLEDGMENTS

O.A. wishes to recognize the financial support of the National Ministry of Education of the Republic of Turkey (Program #: 1416). I.Y. recognizes the financial support of the Ministry of Higher Education of the Arab Republic of Egypt through the Joint Supervision Fellowship Program. I.Y. also recognizes the support of Dr. Ahmed Fadda, Dr. ElSayed Afsah, and Dr. Ibrahim El-Sherbiny for serving as the dissertation committee at Mansoura University, Mansoura, Egypt. The authors thank Dr. Daniel Eitzman and Dr. Jinsang Kim at the University of Michigan for granting access to the Aggro-Link Data Reduction System (Chrono-log Corporation, Havertown, PA) and the QM4 Fluorescence Spectrophotometer (PerkinElmer, Waltham, MA) used to measure platelets aggregation and changes in albumin fluorescence, respectively. The authors also thank Mr. Ahmet Emrehan Emre for his technical assistance with electron microscopy imaging.

REFERENCES

(1) Pazdur, R.; Kudelka, A. P.; Kavanagh, J. J.; Cohen, P. R.; Raber, M. N. The taxoids: paclitaxel (Taxol) and docetaxel (Taxotere). *Cancer Treat. Rev.* **1993**, *19* (4), 351−86.

(2) Abal, M.; Andreu, J. M.; Barasoain, I. Taxanes: microtubule and centrosome targets, and cell cycle dependent mechanisms of action. *Curr. Cancer Drug Targets* **2003**, *3* (3), 193−203.

(3) Schwab, C. L.; English, D. P.; Roque, D. M.; Santin, A. D. Taxanes: their impact on gynecologic malignancy. *Anti-Cancer Drugs* **2014**, *25* (5), 522−535.

(4) FDA approves treatment IND protocol for taxol. *Clin. Pharm.***1992**, *11* (11), 912

(5) Gill, P. S.; Tulpule, A.; Espina, B. M.; Cabriales, S.; Bresnahan, J.; Ilaw, M.; Louie, S.; Gustafson, N. F.; Brown, M. A.; Orcutt, C.; Winograd, B.; Scadden, D. T. Paclitaxel is safe and effective in the treatment of advanced AIDS-related Kaposi's sarcoma. *J. Clin Oncol* **1999**, *17* (6), 1876−83.

(6) Francis, P. A.; Kris, M. G.; Rigas, J. R.; Grant, S. C.; Miller, V. A. Paclitaxel (Taxol) and docetaxel (Taxotere): active chemotherapeutic agents in lung cancer. *Lung Cancer* **1995**, *12* (Suppl. 1), S163−72.

(7) Tankanow, R. M. Docetaxel: a taxoid for the treatment of metastatic breast cancer. *Am. J. Health Syst. Pharm.* **1998**, *55* (17), 1777−91.

(8) Belani, C. P.; Eckardt, J. Development of docetaxel in advanced non-small-cell lung cancer. *Lung Cancer* **2004**, *46* (Suppl. 2), S3−11.

(9) Blagden, S. P.; Kaye, S. B. Docetaxel in the management of ovarian cancer. *Expert Rev. Anticancer Ther.* **2005**, *5* (2), 203−14.

(10) Hagiwara, H.; Sunada, Y. Mechanism of taxane neurotoxicity. *Breast Cancer* **2004**, *11* (1), 82−5.

(11) Markman, M. Managing taxane toxicities. *Support Care Cancer* **2003**, *11* (3), 144−7.

(12) Steele, R. H.; Limaye, S.; Cleland, B.; Chow, J.; Suranyi, M. G. Hypersensitivity reactions to the polysorbate contained in recombinant erythropoietin and darbepoietin. *Nephrology* **2005**, *10* (3), 317−20.

(13) Bergh, M.; Magnusson, K.; Nilsson, J. L.; Karlberg, A. T. Contact allergenic activity of Tween 80 before and after air exposure. *Contact Dermatitis* **1997**, *37* (1), 9−18.

(14) Gelderblom, H.; Verweij, J.; Nooter, K.; Sparreboom, A. Cremophor EL: the drawbacks and advantages of vehicle selection for drug formulation. *Eur. J. Cancer* **2001**, *37* (13), 1590−8.

(15) Gradishar, W. J.; Tjulandin, S.; Davidson, N.; Shaw, H.; Desai, N.; Bhar, P.; Hawkins, M.; O'Shaughnessy, J. Phase III trial of nanoparticle albumin-bound paclitaxel compared with polyethylated castor oil-based paclitaxel in women with breast cancer. *J. Clin. Oncol.* **2005**, *23* (31), 7794−803.

(16) Sempkowski, M.; Locke, T.; Stras, S.; Zhu, C.; Sofou, S. Liposome-Based Approaches for Delivery of Mainstream Chemotherapeutics: Preparation Methods, Liposome Designs. *Crit. Rev. Oncog.* **2014**, *19* (3−4), 177−221.

(17) Peng, Z.-H.; Sima, M.; Salama, M. E.; Kopečková, P.; Kopeček, J. Spacer length impacts the efficacy of targeted docetaxel conjugates in prostate-specific membrane antigen expressing prostate cancer. *J. Drug Targeting* **2013**, *21* (10), 968−980.

(18) Cabral, H.; Kataoka, K. Progress of drug-loaded polymeric micelles into clinical studies. *J. Controlled Release* **2014**, *190* (0), 465−476.

(19) Green, M. R.; Manikhas, G. M.; Orlov, S.; Afanasyev, B.; Makhson, A. M.; Bhar, P.; Hawkins, M. J. Abraxane, a novel Cremophor-free, albumin-bound particle form of paclitaxel for the treatment of advanced non-small-cell lung cancer. *Ann. Oncol* **2006**, *17* (8), 1263−8.

(20) Miele, E.; Spinelli, G. P.; Miele, E.; Tomao, F.; Tomao, S. Albumin-bound formulation of paclitaxel (Abraxane® ABI-007) in the treatment of breast cancer. *Int. J. Nanomed.* **2009**, *4*, 99−105.

(21) Singer, J. W. Paclitaxel poliglumex (XYOTAX, CT-2103): amacromolecular taxane. *J. Controlled Release* **2005**, *109*, 120−126.

(22) Vrignaud, P.; Sémiond, D.; Lejeune, P.; Bouchard, H.; Calvet, L.; Combeau, C.; Riou, J.-F.; Commerçon, A.; Lavelle, F.; Bissery, M.-C. Preclinical Antitumor Activity of Cabazitaxel, a Semisynthetic Taxane Active in Taxane-Resistant Tumors. *Clin. Cancer Res.* **2013**, *19* (11), 2973−2983.

(23) de Bono, J. S.; Oudard, S.; Ozguroglu, M.; Hansen, S.; Machiels, J. P.; Kocak, I.; Gravis, G.; Bodrogi, I.; Mackenzie, M. J.; Shen, L.; Roessner, M.; Gupta, S.; Sartor, A. O. Prednisone plus cabazitaxel or mitoxantrone for metastatic castration-resistant prostate cancer progressing after docetaxel treatment: a randomised open-label trial. *Lancet* **2010**, *376* (9747), 1147−54.

(24) Oudard, S. TROPIC: Phase III trial of cabazitaxel for the treatment of metastatic castration-resistant prostate cancer. *Future Oncol.* **2011**, *7* (4), 497−506.

(25) Paller, C. J.; Antonarakis, E. S. Cabazitaxel: a novel second-line treatment for metastatic castration-resistant prostate cancer. *Drug Des., Dev. Ther.* **2011**, *10* (5), 117−124.

(26) Galletti, E.; Magnani, M.; Renzulli, M. L.; Botta, M. Paclitaxel and docetaxel resistance: molecular mechanisms and development of new generation taxanes. *ChemMedChem* **2007**, *2* (7), 920−42.

(27) Abidi, A. Cabazitaxel: A novel taxane for metastatic castration-resistant prostate cancer-current implications and future prospects. *J. Pharmacol. Pharmacother.* **2013**, *4* (4), 230−237.

(28) Kocherlakota, C.; Banda, N.; Singh, T.; Vure, P.; Biswas, M.; Bhagwatwar, H. P.; Vaya, N.; Khati, N.; Ahmed, S. R., Pharmaceutical formulations of cabazitaxel. *Google Patents*, 2013.

(29) Sanofi-Aventis. JEVTANA® Prescribing Information. Sanofi-Aventis U. S., LLC: Bridgewater, NJ, March 2014.

(30) Norris, L. B.; Qureshi, Z. P.; Bookstaver, P. B.; Raisch, D. W.; Sartor, O.; Chen, H.; Chen, F.; Bennett, C. L. Polysorbate 80 hypersensitivity reactions: a renewed call to action. *Community Oncology* **2010**, *7*, 425−428.

DOI: 10.1021/acs.molpharmaceut.6b00147
Mol. Pharmaceutics 2016, 13, 1413−1429

(31) Matyjaszewski, K.; Xia, J. Atom transfer radical polymerization. *Chem. Rev.* **2001**, *101* (9), 2921−90.
(32) Durmaz, H.; Dag, A.; Altintas, O.; Erdogan, T.; Hizal, G.; Tunca, U. One-Pot Synthesis of ABC Type Triblock Copolymers via in situ Click [3 + 2] and Diels−Alder [4 + 2] Reactions. *Macromolecules* **2007**, *40* (2), 191−198.
(33) Broaders, K. E.; Pastine, S. J.; Grandhe, S.; Frechet, J. M. J. Acid-degradable solid-walled microcapsules for pH-responsive burst-release drug delivery. *Chem. Commun.* **2011**, *47* (2), 665−667.
(34) Shim, M. S.; Kwon, Y. J. Controlled Delivery of Plasmid DNA and siRNA to Intracellular Targets Using Ketalized Polyethylenimine. *Biomacromolecules* **2008**, *9* (2), 444−455.
(35) Lim, H.; Noh, J.; Kim, Y.; Kim, H.; Kim, J.; Khang, G.; Lee, D. Acid-Degradable Cationic Poly(ketal amidoamine) for Enhanced RNA Interference In Vitro and In Vivo. *Biomacromolecules* **2013**, *14* (1), 240−247.
(36) Paramonov, S. E.; Bachelder, E. M.; Beaudette, T. T.; Standley, S. M.; Lee, C. C.; Dashe, J.; Fréchet, J. M. J. Fully Acid-Degradable Biocompatible Polyacetal Microparticles for Drug Delivery. *Bioconjugate Chem.* **2008**, *19* (4), 911−919.
(37) Lee, S. J.; Min, K. H.; Lee, H. J.; Koo, A. N.; Rim, H. P.; Jeon, B. J.; Jeong, S. Y.; Heo, J. S.; Lee, S. C. Ketal Cross-Linked Poly(ethylene glycol)-Poly(amino acid)s Copolymer Micelles for Efficient Intracellular Delivery of Doxorubicin. *Biomacromolecules* **2011**, *12* (4), 1224−1233.
(38) Zhang, A.; Zhang, Z.; Shi, F.; Ding, J.; Xiao, C.; Zhuang, X.; He, C.; Chen, L.; Chen, X. Disulfide crosslinked PEGylated starch micelles as efficient intracellular drug delivery platforms. *Soft Matter* **2013**, *9* (7), 2224−2233.
(39) Medina, S. H.; Chevliakov, M. V.; Tiruchinapally, G.; Durmaz, Y. Y.; Kuruvilla, S. P.; Elsayed, M. E. Enzyme-activated nanoconjugates for tunable release of doxorubicin in hepatic cancer cells. *Biomaterials* **2013**, *34* (19), 4655−66.
(40) Russell, P. J.; Kingsley, E. A. Human prostate cancer cell lines. *Methods Mol. Med.* **2003**, *81*, 21−39.
(41) Pagano, R. E.; Ozato, K.; Ruysschaert, J. M. Intracellular distribution of lipophilic fluorescent probes in mammalian cells. *Biochim. Biophys. Acta, Biomembr.* **1977**, *465* (3), 661−6.
(42) Batrakova, E. V.; Li, S.; Vinogradov, S. V.; Alakhov, V. Y.; Miller, D. W.; Kabanov, A. V. Mechanism of pluronic effect on P-glycoprotein efflux system in blood-brain barrier: contributions of energy depletion and membrane fluidization. *J. Pharmacol. Exp. Ther.* **2001**, *299* (2), 483−93.
(43) Lin, Y. L.; Jiang, G.; Birrell, L. K.; El-Sayed, M. E. Degradable, pH-sensitive, membrane-destabilizing, comb-like polymers for intracellular delivery of nucleic acids. *Biomaterials* **2010**, *31* (27), 7150−66.
(44) Jurasz, P.; Alonso, D.; Castro-Blanco, S.; Murad, F.; Radomski, M. W. Generation and role of Angiostatin in human platelets. *Blood* **2003**, *102* (9), 3217−23.
(45) Radomski, A.; Stewart, M. W.; Jurasz, P.; Radomski, M. W. Pharmacological characteristics of solid-phase von Willebrand factor in human platelets. *Br. J. Pharmacol.* **2001**, *134* (5), 1013−20.
(46) Radomski, A.; Jurasz, P.; Alonso-Escolano, D.; Drews, M.; Morandi, M.; Malinski, T.; Radomski, M. W. Nanoparticle-induced platelet aggregation and vascular thrombosis. *Br. J. Pharmacol.* **2005**, *146* (6), 882−93.
(47) Suk, J. S.; Xu, Q.; Kim, N.; Hanes, J.; Ensign, L. M. PEGylation as a strategy for improving nanoparticle-based drug and gene delivery. *Adv. Drug Delivery Rev.* **2016**, *99*, 28−51.
(48) Ge, J.; Neofytou, E.; Lei, J.; Beygui, R. E.; Zare, R. N. Protein−Polymer Hybrid Nanoparticles for Drug Delivery. *Small* **2012**, *8* (23), 3573−3578.
(49) Bettencourt, A.; Almeida, A. J. Poly(methyl methacrylate) particulate carriers in drug delivery. *J. Microencapsulation* **2012**, *29* (4), 353−67.
(50) Chen, L. Hydrogel/Polymer Micelles Composites Derived from Polymerization of Microemulsions for Oral Drug Delivery. University of Akron: 2013.
(51) Feng, Z.; Bo, Y. Polymer Brushes on Surfaces. In *Self-Assembled Structures*; CRC Press: 2010; pp 175−207.
(52) Lee, R.-S.; Huang, Y.-T. Tuning the hydrophilic-hydrophobic balance of block-graft copolymers by click strategy: synthesis and characterization of amphiphilic PCL-b-(P[alpha]N3CL-g-PBA) copolymers. *Polym. J.* **2010**, *42* (4), 304−312.
(53) Oerlemans, C.; Bult, W.; Bos, M.; Storm, G.; Nijsen, J. F.; Hennink, W. E. Polymeric micelles in anticancer therapy: targeting, imaging and triggered release. *Pharm. Res.* **2010**, *27* (12), 2569−89.
(54) Gillies, E. R.; Jonsson, T. B.; Frechet, J. M. Stimuli-responsive supramolecular assemblies of linear-dendritic copolymers. *J. Am. Chem. Soc.* **2004**, *126* (38), 11936−43.
(55) Sackett, D. L.; Wolff, J. Nile red as a polarity-sensitive fluorescent probe of hydrophobic protein surfaces. *Anal. Biochem.* **1987**, *167* (2), 228−34.
(56) Chen, J.; Qiu, X.; Ouyang, J.; Kong, J.; Zhong, W.; Xing, M. M. pH and reduction dual-sensitive copolymeric micelles for intracellular doxorubicin delivery. *Biomacromolecules* **2011**, *12* (10), 3601−11.
(57) Lee, S. C.; Huh, K. M.; Lee, J.; Cho, Y. W.; Galinsky, R. E.; Park, K. Hydrotropic Polymeric Micelles for Enhanced Paclitaxel Solubility: In Vitro and In Vivo Characterization. *Biomacromolecules* **2007**, *8* (1), 202−208.
(58) Wei, R.; Cheng, L.; Zheng, M.; Cheng, R.; Meng, F.; Deng, C.; Zhong, Z. Reduction-responsive disassemblable core-cross-linked micelles based on poly(ethylene glycol)-b-poly(N-2-hydroxypropyl methacrylamide)-lipoic acid conjugates for triggered intracellular anticancer drug release. *Biomacromolecules* **2012**, *13* (8), 2429−38.
(59) You, J.; Hu, F. Q.; Du, Y. Z.; Yuan, H. Polymeric micelles with glycolipid-like structure and multiple hydrophobic domains for mediating molecular target delivery of paclitaxel. *Biomacromolecules* **2007**, *8* (8), 2450−6.
(60) Soleymani Abyaneh, H.; Vakili, M. R.; Lavasanifar, A. The effect of polymerization method in stereo-active block copolymers on the stability of polymeric micelles and their drug release profile. *Pharm. Res.* **2014**, *31* (6), 1485−500.
(61) Yang, C.; Attia, A. B.; Tan, J. P.; Ke, X.; Gao, S.; Hedrick, J. L.; Yang, Y. Y. The role of non-covalent interactions in anticancer drug loading and kinetic stability of polymeric micelles. *Biomaterials* **2012**, *33* (10), 2971−9.
(62) Read, E. S.; Armes, S. P. Recent advances in shell cross-linked micelles. *Chem. Commun. (Cambridge, U. K.)* **2007**, *29*, 3021−35.
(63) Shen, Y. *Functional polymers for nanomedicine*; Royal Society of Chemistry: Cambridge, 2013; p 1 online resource (xii, 318 pp).
(64) Fang, J.; Nakamura, H.; Maeda, H. The EPR effect: Unique features of tumor blood vessels for drug delivery, factors involved, and limitations and augmentation of the effect. *Adv. Drug Delivery Rev.* **2011**, *63* (3), 136−51.
(65) Montaudon, D.; Vrignaud, P.; Londos-Gagliardi, D.; Robert, J. Fluorescence anisotropy of cell membranes of doxorubicin-sensitive and -resistant rodent tumoral cells. *Cancer Res.* **1986**, *46* (11), 5602−5.
(66) Fuchs, P.; Parola, A.; Robbins, P. W.; Blout, E. R. Fluorescence polarization and viscosities of membrane lipids of 3T3 cells. *Proc. Natl. Acad. Sci. U. S. A.* **1975**, *72* (9), 3351−4.
(67) de Laat, S. W.; van der Saag, P. T.; Shinitzky, M. Microviscosity modulation during the cell cycle of neuroblastoma cells. *Proc. Natl. Acad. Sci. U. S. A.* **1977**, *74* (10), 4458−61.
(68) Ramu, A.; Glaubiger, D.; Weintraub, H. Differences in lipid composition of doxorubicin-sensitive and -resistant P388 cells. *Cancer Treat. Rep.* **1984**, *68* (4), 637−41.
(69) Dobrovolskaia, M. A.; Aggarwal, P.; Hall, J. B.; McNeil, S. E. Preclinical studies to understand nanoparticle interaction with the immune system and its potential effects on nanoparticle biodistribution. *Mol. Pharmaceutics* **2008**, *5* (4), 487−95.
(70) Moghimi, S. M.; Hunter, A. C.; Murray, J. C. Long-circulating and target-specific nanoparticles: theory to practice. *Pharmacol Rev.* **2001**, *53* (2), 283−318.
(71) Kim, D.; El-Shall, H.; Dennis, D.; Morey, T. Interaction of PLGA nanoparticles with human blood constituents. *Colloids Surf., B* **2005**, *40* (2), 83−91.

DOI: 10.1021/acs.molpharmaceut.6b00147
Mol. Pharmaceutics 2016, 13, 1413−1429

(72) Gaw, A. *Clinical biochemistry: an illustrated colour text*; Churchill Livingstone: Edinburgh; New York, 2008; p vii, 179 pp.

DOI: 10.1021/acs.molpharmaceut.6b00147
Mol. Pharmaceutics 2016, 13, 1413−1429